NIST Special Publication 260-175

Standard Reference Materials:

SRM 1453, Expanded Polystyrene Board, for Thermal Conductivity from 281 K to 313 K

Robert R. Zarr
Adam L. Pintar

http://dx.doi.org/10.6028/NIST.SP.260-175

National Institute of Standards and Technology
U.S. Department of Commerce

NIST Special Publication 260-175

Standard Reference Materials:

SRM 1453, Expanded Polystyrene Board, for Thermal Conductivity from 281 K to 313 K

Robert R. Zarr
Energy and Environment Division
Engineering Laboratory

Adam L. Pintar
Statistical Engineering Division
Information Technology Laboratory

http://dx.doi.org/10.6028/NIST.SP.260-175

December 2012

U.S. Department of Commerce
Rebecca Blank, Acting Secretary

National Institute of Standards and Technology
Patrick D. Gallagher, Under Secretary of Commerce for Standards and Technology and Director

National Institute of Standards and Technology Special Publication 260-175
Natl. Inst. Stand. Technol. Spec. Publ. 260-175, 57 pages (December 2012)
http://dx.doi.org/10.6028/NIST.SP. 260-175
CODEN: NSPUE2

Authors' Note: This document is based on NISTIR 5838, *Room-Temperature Thermal Conductivity of Expanded Polystyrene Board for a Standard Reference Material* (May 1996). Most of the content remains the same; the thermal conductivity data and the corresponding uncertainty analysis have been updated to reflect recent modifications in the heat flow determination. The statistical analysis of the data has been updated following an errors-in-variables approach. In addition, the terminology has been updated in conformance with current documentary standards for the guarded-hot-plate test method.

Abstract

Thermal conductivity measurements at and near room temperature are presented as the basis for certified values of thermal conductivity of SRM 1453, Expanded Polystyrene Board. The measurements have been conducted in accordance with a randomized full factorial experimental design with two variables, bulk density and temperature, using the NIST 1016 mm line-heat-source guarded hot plate apparatus. The thermal conductivity measurements were conducted over a range of bulk density from 37.4 kg/m^3 to 45.8 kg/m^3 and mean temperature from 281 K to 313 K. Uncertainties of the measurements, consistent with current ISO guidelines, have been developed. Statistical analyses of the physical properties of the SRM are presented and include variations between boards, as well as within boards. Measurements of the foam surface roughness, microstructure, and compressive resistance are presented.

Each unit of SRM 1453 is batch certified for thermal conductivity with the following equation:

$$\lambda = 0.00111 - 0.000\,042\,4\,\rho + 0.000\,115\,T_m$$

where λ is the predicted thermal conductivity (W/(m·K)), ρ is the bulk density (kg/m^3) and, T_m is the mean temperature (K) valid over the bulk density and temperature ranges of 37 kg/m^3 to 46 kg/m^3 and 281 K to 313 K, respectively. The expanded uncertainty for λ is 1.5 % with a coverage factor of approximately $k = 2$.

Keywords

calibration; bulk density; expanded polystyrene board; fenestration; guarded-hot-plate apparatus; heat-flow-meter apparatus; standard reference material; SRM 1453; thermal conductivity; thermal insulation; uncertainty

Table of Contents

1. Introduction

In general, a Standard Reference Material®[1] (SRM) issued by the National Institute of Standards and Technology (NIST) is a homogeneous and stable material which is measured accurately and certified as a reference material for purposes of evaluating a measurement process [1]. Standard Reference Materials are provided by NIST as primary tools to assist user communities in achieving measurement quality assurance and metrological traceability. These materials are used by industry, academia, and government to verify or improve the accuracy of specific measurements and to advance the state-of-the-art knowledge. New SRMs are developed, usually after a formal request, in order to satisfy the measurement needs of a user community.

1.1 Thermal Insulation SRMs

Thermal insulation SRMs are issued by NIST for materials with certified value assignments for thermal resistance and thermal conductivity over a range of parameters, such as bulk density and temperature. These SRMs are utilized in standard test methods for the purposes of checking guarded-hot-plate apparatus [2], calibrating heat-flow-meter apparatus [3], and, when necessary, for checking or calibrating hot-box apparatus [4]. The systematic use of thermal insulation SRMs, including proper tracking with control charts, provides the means for accurate inter-laboratory comparison of thermal conductivity data.

Value assignments for thermal insulation SRMs issued by NIST are developed using the guarded-hot-plate method [2]. The method is considered an absolute measurement procedure because the resulting thermal transmission properties are determined directly from basic measurements of length, area, temperature, and electrical power. Essentially, the method establishes steady-state heat flow through flat homogeneous slabs – the surfaces of which are in contact with adjoining parallel boundaries (i.e., plates) maintained at constant temperatures. By accurately monitoring the plate separation and knowing the geometric shape factor for the heat flow, the steady-state heat transmission properties of the test specimen are determined using the Fourier heat conduction equation. Influence quantities such as plate clamping pressure, plate emittance, and ambient air temperature, among others, are controlled; while other quantities such as ambient air pressure are monitored during the measurement process. In principle, the method can be used over a wide range of insulating materials, mean temperatures, and temperature differences.

The thermal resistance and thermal conductivity of a thermal insulation SRM are generally characterized as functions of bulk density and mean temperature. The characterization is typically accomplished by batch certification. A sampling scheme is used to select specific specimens from the material lot for testing in the guarded-hot-plate apparatus. The analysis of the thermal conductivity data of the sample sub-lot is used for certification of the SRM lot. Consequently, the uncertainty statement for a thermal insulation SRM contains a component of uncertainty (usually small) due to the material lot variability. It should be noted that a thermal insulation SRM unit issued to a customer has not been measured directly in a NIST guarded-hot-plate apparatus. The advantage of the

[1] The term "Standard Reference Material" and the diamond-shaped logo which contains the term "SRM," are registered with the United States Patent and Trademark Office.

batch approach is realized by characterizing a large quantity of units that are economical and available on demand. In practice, thermal insulation SRM lots are prepared with a sufficient number of units to meet anticipated demand for a period of ten years.

Standard Reference Material 1453 is a rigid, high-density, molded expanded polystyrene board that was fabricated from a single production run by a commercial manufacturer of molded polystyrene foam products. Standard Reference Material 1453 is one of several certified thermal insulation reference materials issued by NIST. These related thermal insulation SRMs have been categorized by the NIST Standard Reference Materials Program (SRMP) in *Table 203.17 – Thermal Resistance and Thermal Conductivity Properties of Glass, Silica, and Polystyrene (solid forms)* reproduced in Table 1.

Table 1. Thermal resistance and thermal conductivity of glass, silica, and polystyrene

Designation	Description	Temperature range (K)
1449	Fumed silica board	297.1
1450d	Fibrous glass board	280 to 340
1452	Fibrous glass blanket	297.1 (100 to 330)
1453	Expanded polystyrene board	285 to 310
1459	Fumed silica board	297.1

NIST Special Publication 260-175 (this publication), which is part of the "NIST Special Publication 260 Series," provides supplemental documentation for the 1453 Certificate and covers the following subject matter:

1) historical background of SRM 1453;
2) project plan for certification including the fabrication and procurement of the material lot;
3) measurement methods for the bulk density and thermal conductivity evaluations;
4) uncertainty analysis; and,
5) certification.

1.2 Historical Background

The motivation for SRM 1453, Expanded Polystyrene Board, began in the late 1980s during the development of the ASTM Test Method C1199 [4] for the thermal evaluation of fenestration systems. The test method requires the use of a large calibration transfer standard having known thermal transmission properties in order to estimate the surface heat transfer coefficients of more complex fenestration systems. The motivation increased when the Energy Policy Act of 1992 [5] mandated that a voluntary window rating program be developed by the National Fenestration Rating Council (NFRC) according to accepted national testing procedures.

On March 11, 1993, representatives from NFRC, industry, and the National Voluntary Laboratory Accreditation Program (NVLAP) met at the National Institute of Standards and Technology (NIST) to discuss, among other topics, a proposal for a new SRM. The primary purpose of the new SRM would be to assist the thermal testing community in the thermal evaluation of fenestration systems, especially windows. The meeting representatives discussed the criteria for the new SRM with regards to the design requirements for

the calibration transfer standard. The design for the transfer standard was based on work done at the National Research Council of Canada [6] and consisted of 13-mm thick expanded polystyrene foam (20 kg/m^3) bonded, on both sides, to 3 mm glass sheets [7].

Preliminary measurements were conducted by NIST on similar specimens of molded expanded polystyrene foam provided for this purpose by insulation manufacturers. The bulk density of the specimens ranged from 41 kg/m^3 to 49 kg/m^3 and the average thermal conductivity (at 24 °C) for the specimens was 0.033 W/(m·K). The effect of density on thermal conductivity was found to be fairly insensitive for boards about 13 mm in thickness. Based on these preliminary studies, NIST procured a large number of boards of molded expanded polystyrene foam for production of SRM 1453.

2. Certification Project Design

2.1 Project Definition and Scope for Intended Use

The certification project is defined as follows.

> "*The preparation of thermal insulation SRM 1453 for thermal resistance and thermal conductivity measurements with expanded uncertainties (k = 2) associated with the certified values of less than or equal to 2 % over a mean temperature range of 281 K to 313 K.*"

Standard Reference Material 1453 is intended for use as a proven check for the guarded-hot-plate apparatus, hot box apparatus (or other absolute thermal conductivity apparatus), and for calibration of a heat-flow-meter apparatus over the temperatures 280 K to 340 K. This report cannot exclude the use of SRM 1453 for other purposes, but the user is cautioned that other purposes are not necessarily covered by the 1453 Certificate or by this report. Additional usage issues are covered in Sec. 7.3.4 and in the 1453 Certificate (under Instructions For Handling, Storage, And Use).

2.2 Material

Standard Reference Material 1453 is a commercial rigid, high-density, molded expanded polystyrene board. The nominal physical properties of the material are as follows:

- size: 660 mm by 930 mm
- thickness: 13 mm
- bulk density: 41 kg/m^3

2.2.1 Fabrication

NIST purchased 300 boards of molded polystyrene foam from Polyfoam, Incorporated[2] in April 1994. The foam beads were manufactured by expanding (under heating conditions) particles of a polystyrene polymer saturated with a volatile hydrocarbon, such as isopentane. The expanded beads were subsequently placed in a plank mold and heated under pressure until the beads fused together.

2.2.2 Surface Preparation

To remove surface imprints from the molding process, the boards were shipped directly to a second vendor (Rollin Incorporated[2]) where both sides of each board were sanded using a modified milling machine in order to obtain a uniform thickness. The final nominal dimensions of the sanded boards were 660 mm by 930 mm by 13 mm thick.

2.2.3 Delivery

The boards were delivered to NIST on November 10, 1994, and placed in a storage room maintained at 21 °C ± 2 °C and a relative humidity that ranged from 30 % to 60 %.

[2] Certain commercial equipment, instruments, or materials are identified in this report to specify adequately the experimental procedure. Such identification does not imply recommendation or endorsement by NIST, nor does it imply that the materials or equipment are necessarily the best for the purpose.

2.3 Project Design Plan

The schematic in Figure 1 outlines the project plan for the development and production of SRM 1453, Expanded Polystyrene Board. The experimental portion of the plan, including the selection of test specimens, was based on an experimental design provided by the NIST Statistical Engineering Division.

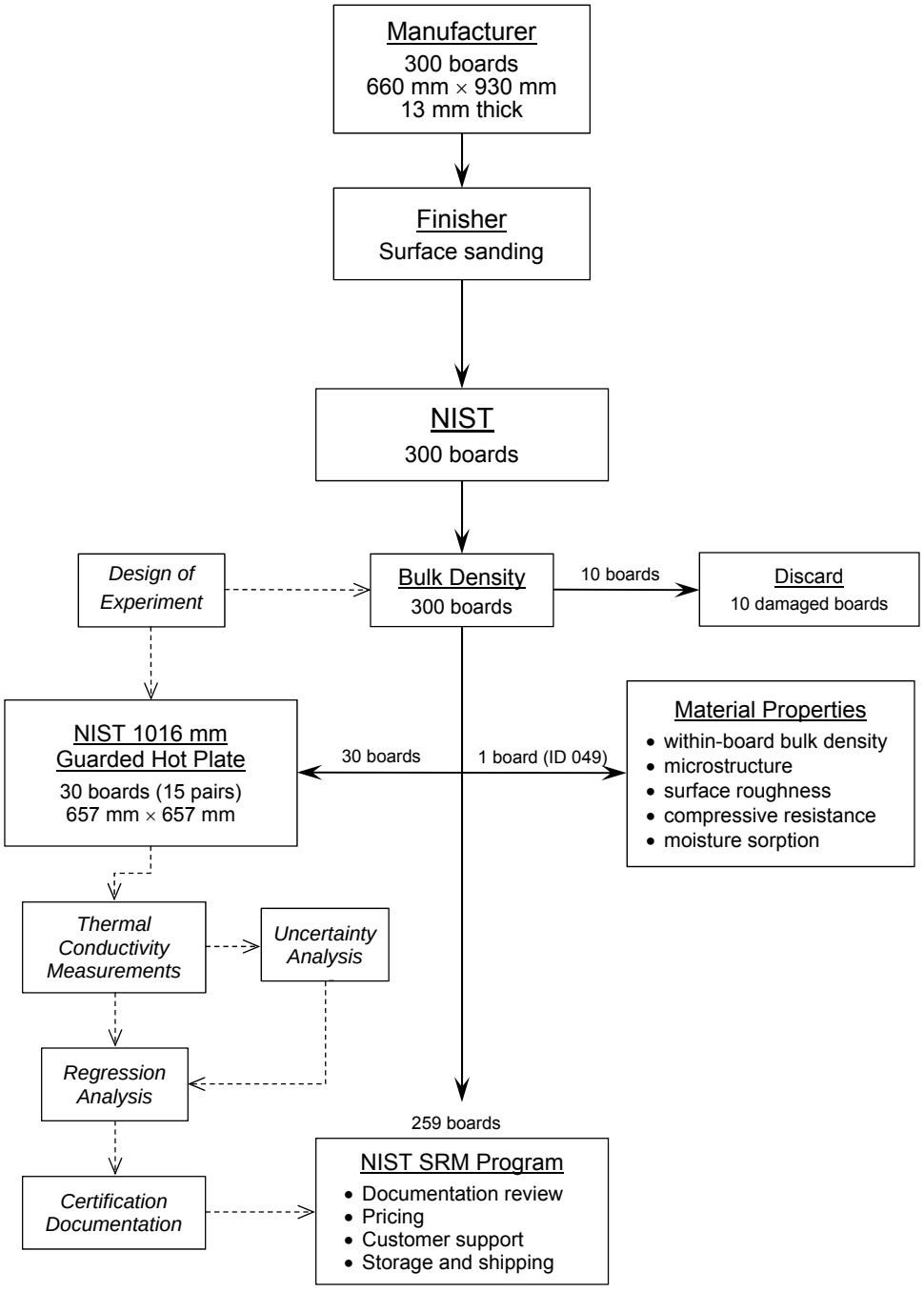

Figure 1. Certification project plan for NIST SRM 1453, Expanded Polystyrene Board

2.3.1 Inspection and Storage

The insulation boards were visually inspected for damage after delivery. Each board was identified with a temporary 3-digit number assigned from 001 to 300. The material lot was stored for several months in laboratory workspace at ambient conditions.

2.3.2 General Sampling Procedure

The sampling plan was based on the certification project plan shown in Fig. 1 and, in particular, on the experiment design referred to as part of the project plan. For 100 % sampling of the material lot, the boards were individually removed from their shipping box containers for mass and dimensional measurements. The 300 boards were processed through a two-day measurement procedure described in Sec. 2.4.1.

2.4 Measurement Methods

2.4.1 Bulk Density

The bulk density, as defined in ASTM Test Method C 177 [2], was determined for each individual finished board from established gravimetric and dimensional measurement procedures that are described in Sec. 3. The major objective of the bulk density study is to assess the material variability of the material lot (i.e., variability between insulation boards), thereby providing quantitative information for the following:

- quantitative ranking of the material lot by bulk density;
- the upper and lower bulk density limits of the material lot; and,
- the detection of any anomalous thermal insulation boards for possible exclusion.

2.4.2 Steady-State Thermal Transmission Properties

The steady-state thermal transmission measurements (i.e., thermal conductivity and thermal resistance) were determined in accordance with ASTM Test Method C 177 [2] using the NIST 1016 mm guarded-hot-plate apparatus. In contrast to the 100 % sampling process for the bulk density study, the thermal conductivity of 1453 was batch certified. The material lot was sub-sampled (Fig. 1) using 30 boards (15 pairs) at three levels of bulk density (low, mid, and high). The quantitative values for these density rankings were defined using the results of the bulk density study (Sec. 3). Detailed procedures of the guarded-hot-plate test method, apparatus, corresponding uncertainty, and thermal characterization are documented in Sec. 4-5.

2.4.3 Supplementary Measurements

Figure 1 outlines supplementary measurements for material properties that were not part of the certification process for SRM 1453. These measurements were intended to provide further insight about the statistical characterization of the material lot and include the following:

- within-board bulk density analysis;
- microstructure using a scanning electron microscope;
- surface roughness using a contact (stylus) profilometer;
- compressive resistance; and,
- moisture sorption using fixed-point humidities.

3. Material Properties

Section 3 describes the physical properties of the material lot, including density variations between boards and within one board, cellular microstructure, and surface profile.

3.1 Bulk Density of Material Lot

The bulk density for a board (ρ_b, kg/m^3) was determined from gravimetric and dimensional measurements of the board using Eq. (1).

$$\rho_b = \frac{m_b}{A_b \times L_b} = \frac{m_b}{l_{1b} \times l_{2b} \times L_b} \tag{1}$$

where the subscript b refers to the expanded polystyrene board, m_b is the mass of the board (kg); A_b is the area of the board (m^2) as determined by length and width dimensions (l_{1b} and l_{2b}, respectively); and, L_b is the board thickness (m). The mass (m_b) of the insulation board was measured by a digital weighing balance (32.1 kg range, 0.0001 kg resolution). Dimensional measurements l_{ib} (i = 1,2) and L_b were determined using a steel rule (0.05 mm resolution) and hand calipers (0.01 mm resolution), respectively.

3.1.1 Graphical Analysis of L_b and ρ_b Data

Variations in L_b and ρ_b (board-to-board) were analyzed graphically using a four-step method. The method consisted of 1) a run-sequence plot that checked for systematic and random changes; 2) a lag plot that checked for randomness; 3) a histogram that checked the frequency distribution; and, 4) a normal probability (normality) plot that checked for the normality assumption. Examples of the method are illustrated in Figs. 2 and 3 for L_b and ρ_b, respectively.

The data in Fig. 2 reveal that, with the exception of five boards greater than 13.5 mm, the thickness of the 300 boards is, in general, very consistent from board to board. The presence of a few tail (extreme end) points is routinely observed with empirical data. The distribution of thicknesses is random as shown by the tight cluster ("bull's-eye") of data points in the center of the lag plot. The distribution is approximately normally distributed as shown in the histogram and normality plot about a sample mean value of 13.23 mm.

In Fig. 3, there are suggestions of multimodality, that is, two or more underlying populations of bulk density each with a single peak. This is noticeable in the run sequence plot (Fig. 3a) and the lag plot (Fig. 3b). The run sequence plot reveals high/low excursions from the mean values and the lag plot reveals localized clusters of data points indicating that the distribution of data is skewed, particularly toward the lower bulk densities. The multimodality is evident in the histogram which confirms this observation and shows two peaks, a large peak at about 39 kg/m^3 and a smaller peak near 43 kg/m^3. The normality plot (Fig. 3d) identified Board 049 for supplemental tests.

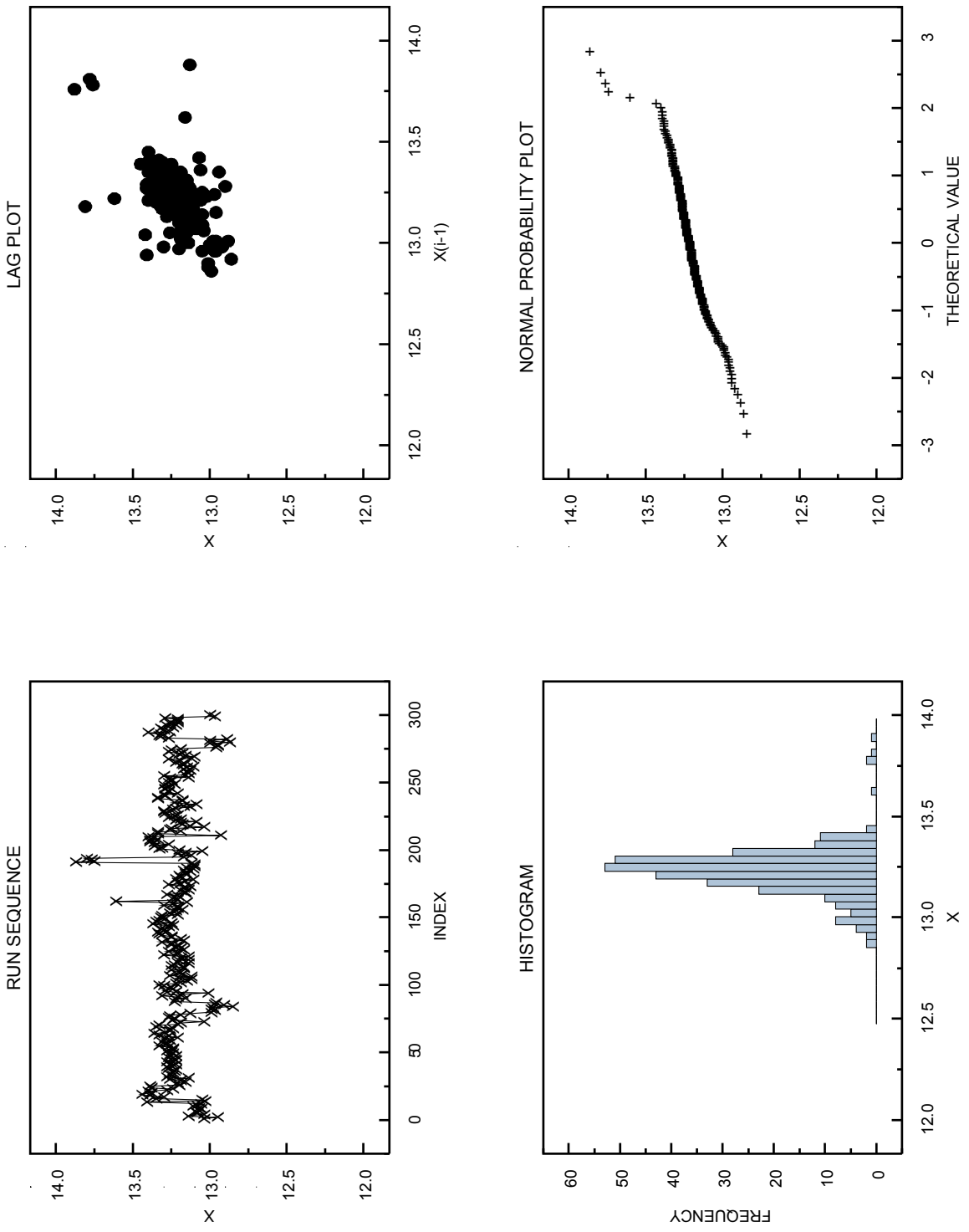

Figure 2. Graphical analysis of board thickness (n = 300): (a) run sequence plot, (b) lag plot, (c) histogram, (d) normal probability plot (normality index). Summary statistics: sample mean = 13.23 mm, sample standard deviation = 0.13 mm.

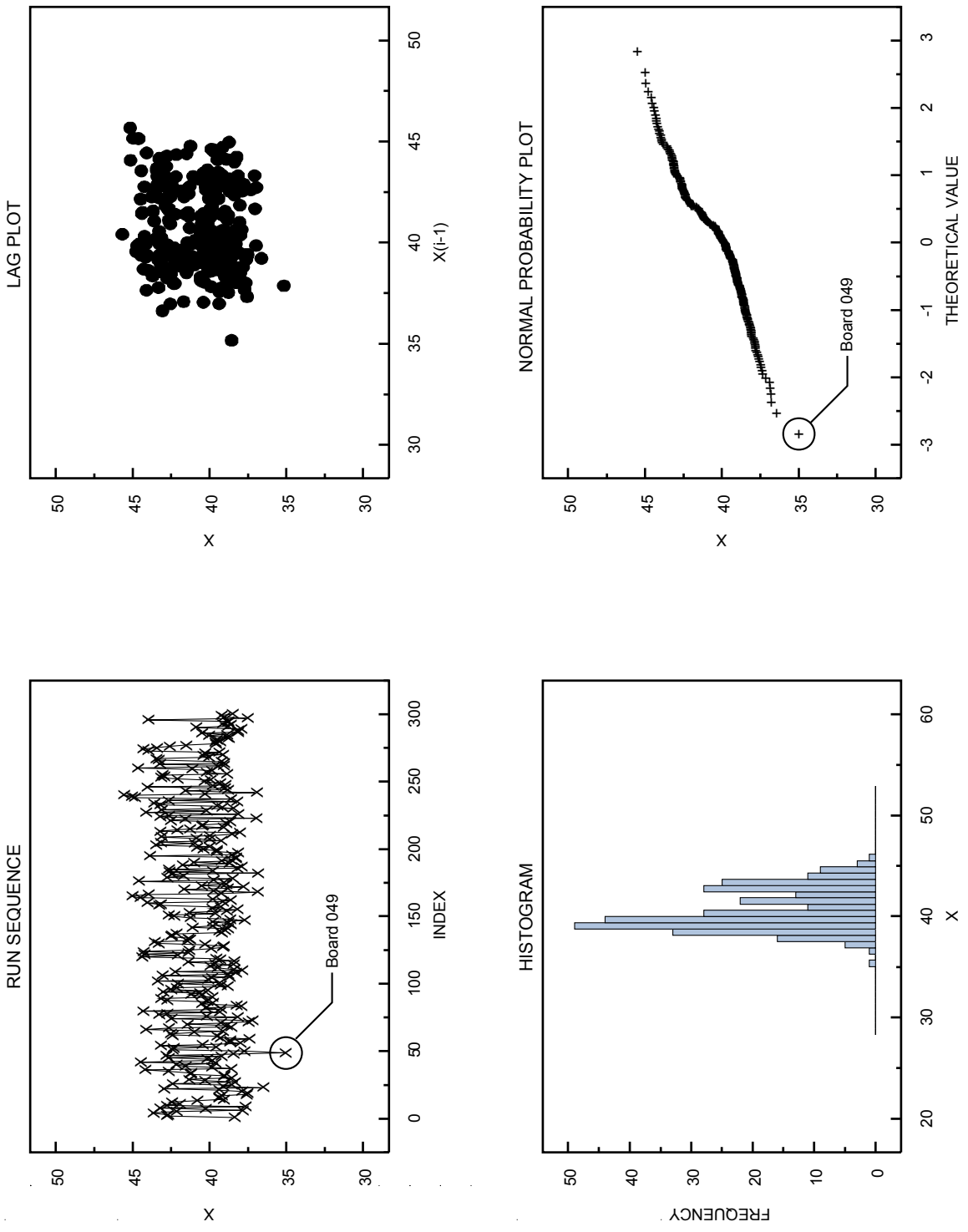

Figure 3. Graphical analysis of bulk density (n = 300): (a) run sequence plot, (b) lag plot, (c) histogram, (d) normal probability plot (normality index). Summary statistics: sample mean = 40.60 kg/m^3, sample standard deviation = 2.05 kg/m^3.

3.1.2 Summary Statistics for Material Lot

Table 2 presents summary statistics for the mass, length, width, thickness, and bulk density of the 300 boards. Overall values for length and width are within acceptable limits (nominally 931 mm by 657 mm). The large range and small standard deviation for thickness indicate that some of the panels are somewhat oversized in thickness (Fig. 2). The bulk density mean and standard deviation values are acceptable.

Table 2. Summary statistics for the SRM 1453 production run (300 boards)

	Mass (g)	Length (mm)	Width (mm)	Thickness (mm)	Bulk density (kg/m^3)
Mean	328.3	930.7	656.9	13.23	40.6
Std. dev.	16.9	0.4	1.3	0.13	2.1
Maximum	371.1	931.5	658.0	13.88	45.7
Minimum	285.1	927.5	636.5	12.86	35.2

Board 049 was identified as having a particularly low density (Fig. 3), removed from the lot, and utilized for supplemental measurements that included within-board density analysis, scanning electron microscopy, and surface profile measurements (Sec. 3.2-3.4).

3.2 Bulk Density within a Board

The density variation with respect to position within a board was examined by cutting Board 049 into 35 specimens, each 127 mm by 127 mm, as illustrated in Fig. 4. The bulk densities, $\rho_{049\text{-}01}$ through $\rho_{049\text{-}35}$, were determined using Eq. (1) and the resulting data were analyzed graphically in Fig. 5 using the four-step method described in Sec. 3.1.1.

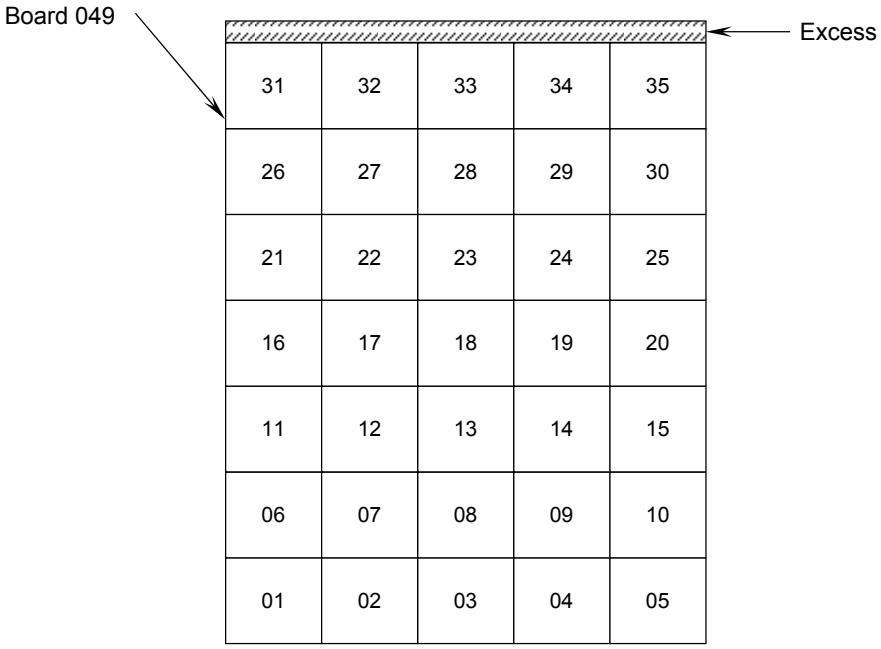

Figure 4. Diagram of Board 049 sampling plan (not to scale)

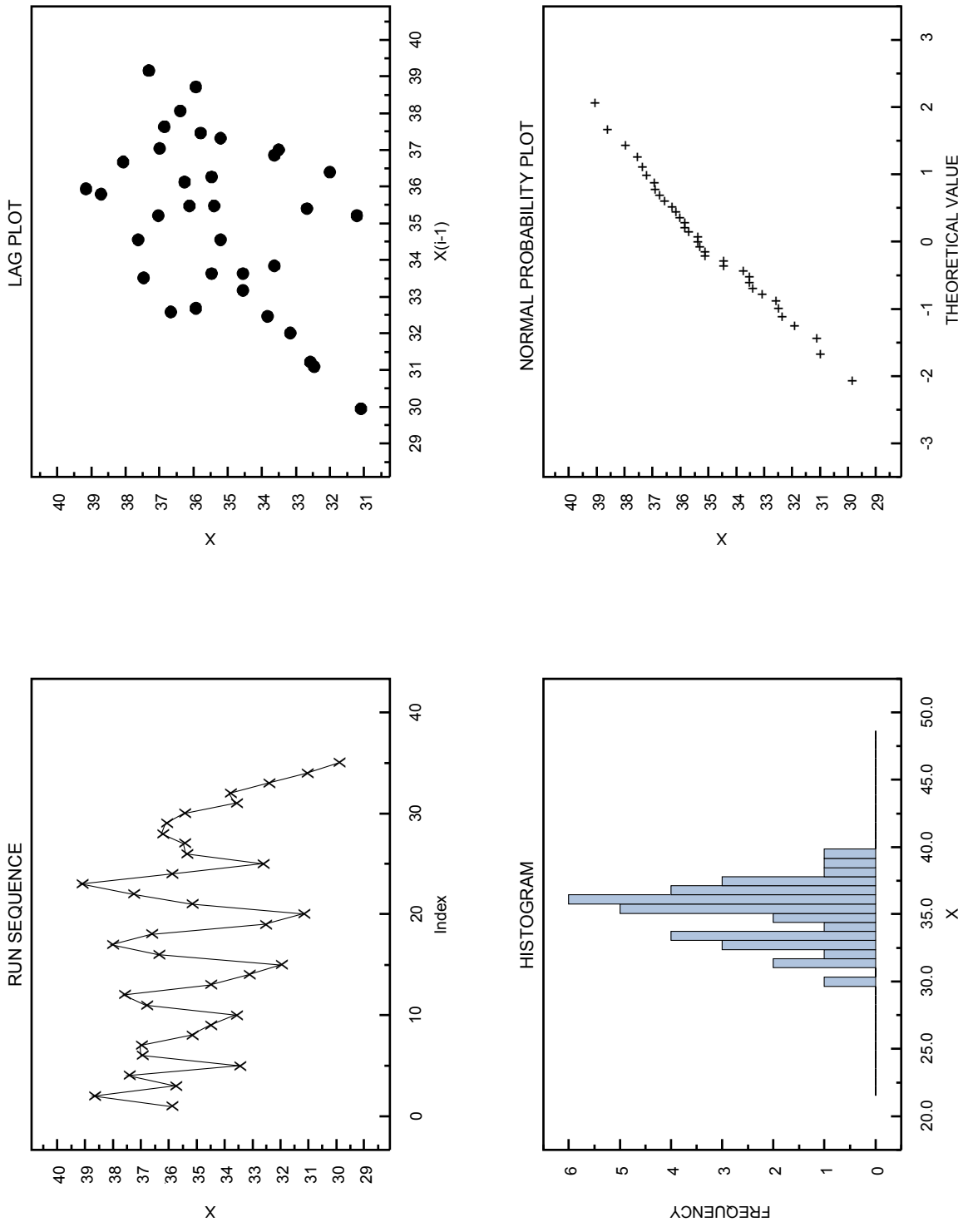

Figure 5. Graphical analysis of bulk density measurements (n = 35) from Board 049: (a) run sequence plot, (b) lag plot, (c) histogram, (d) normal probability plot (normality index). Summary statistics: sample mean = 35.09 kg/m^3, sample standard deviation = 2.26 kg/m^3.

The histogram in Fig. 5c reveals a large peak near 36 kg/m^3 and a small peak near 33 kg/m^3. The mean bulk density for Board 049 was 35.09 kg/m^3 (only slightly lower than the minimum value in Table 2) and the standard deviation was 2.26 kg/m^3.

The cyclic pattern in Fig. 5a is an artifact of the run order (01-35) shown in Fig. 4. The variation of bulk density within Board 049 is illustrated with the contour plot shown in Fig. 6. The higher values of bulk density were located near the center of the board; the lower values of bulk density near the edges and corners.

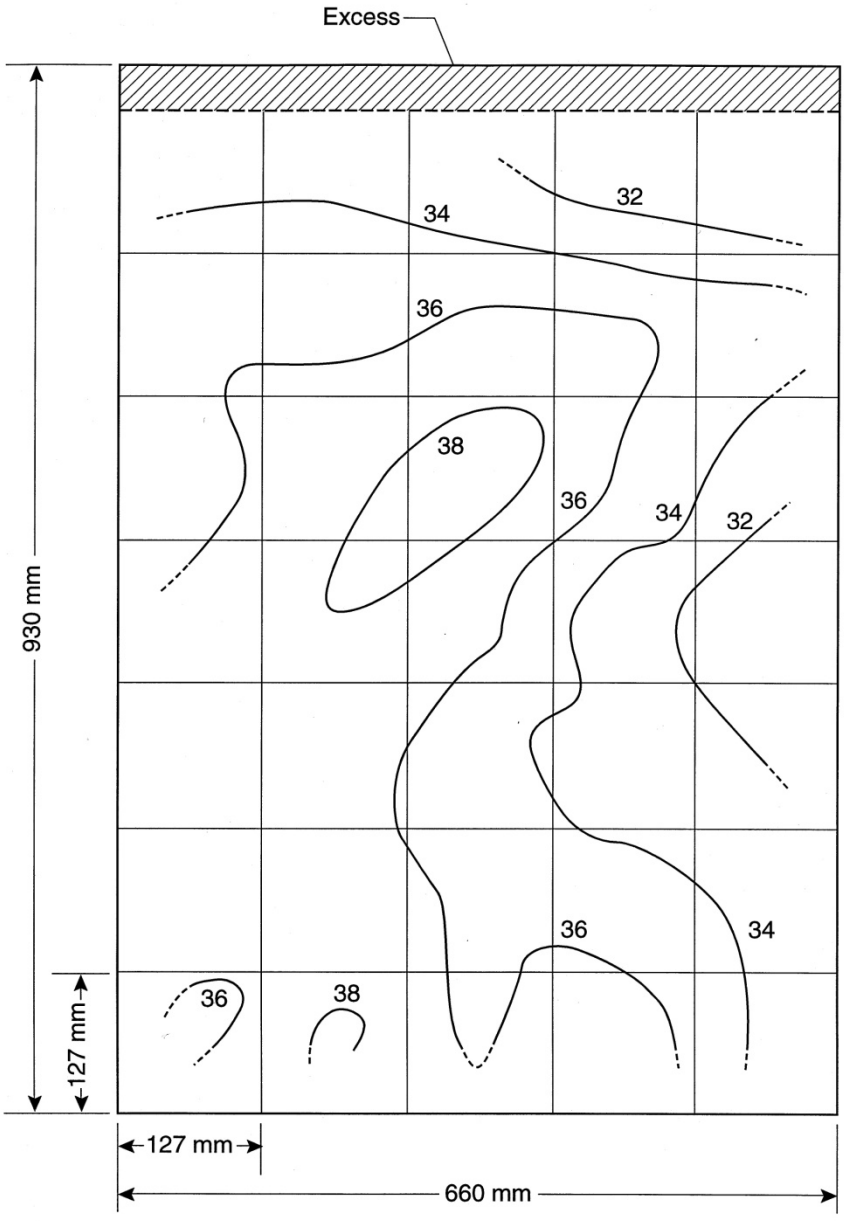

Figure 6. Contour plot of bulk density (in kg/m^3) for Board 049.

3.3 Microstructure

The microcellular structure of the foam was examined using scanning electron microscopy (SEM). Small samples of foam, approximately 5 mm by 13 mm by 28 mm, were cut from one board using a razor blade and were subsequently sputter-coated with a 20 nm film of gold to prevent surface charging. Secondary electron images of the surface topography were obtained under operating conditions of 4 keV and a current of about 500 pA. Two images of the foam, at magnifications of 25× and 100×, are shown in Figs. 7a and 7b, respectively.

The SEM micrograph in Fig. 7a (magnification 25×) shows the interfacial outlines of the fused beads of expanded polystyrene from the molding process. The size of the beads ranged from 1 mm to 3 mm and the voids at the intersection of three or more beads, if present, were relatively small as noted in the micrograph. Figure 7b (magnification 100×) reveals the distribution of microcells formed within the beads during the initial expansion process. The cells, which are somewhat elliptical in shape, have major diameter lengths ranging from 0.02 mm to 0.4 mm. As evident in the micrograph, a large percentage of the cell walls were intact indicating a relatively high content of closed cells.

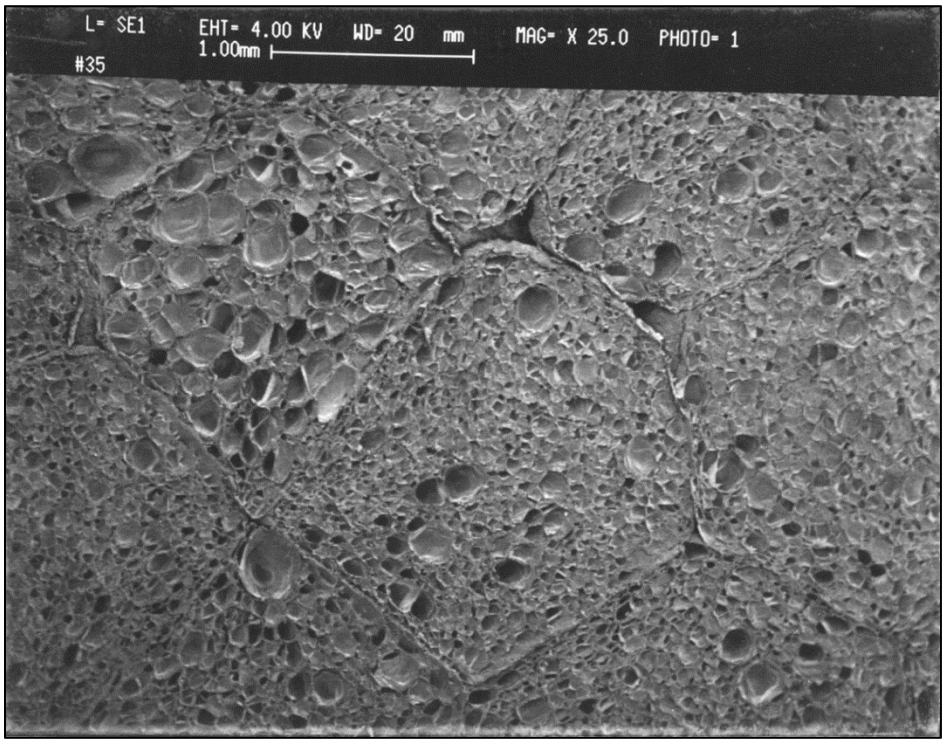

Figure 7a. SEM micrograph (25×) shows outlines of molded beads and internal cellular structure

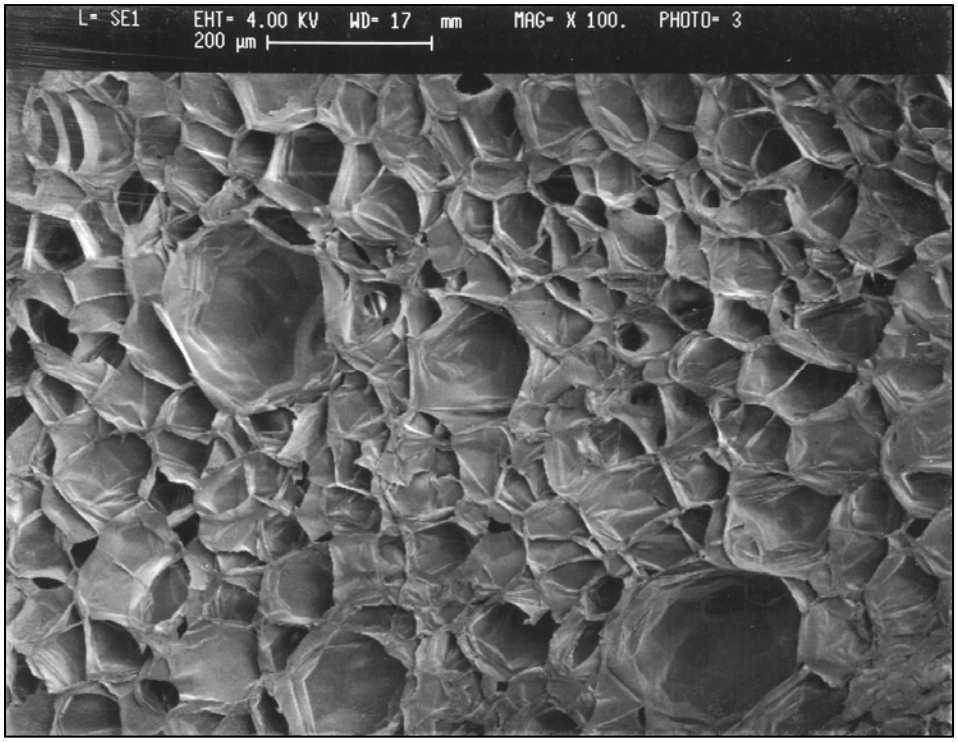

Figure 7b. SEM micrograph (100×) shows close-up of cellular structure

3.4 Surface Roughness

The surface roughness of the foam was examined by the NIST Precision Engineering Division with a contact profilometer (Form Talysurf[1] instrument) that generated a surface profile by means of a contact stylus. Sub-specimen 21 from Board 049 (Fig. 4) was securely fastened relative to the instrument's stylus. The stylus was traversed over a sampling interval of the foam at three different locations. Displacements of the stylus in the *z*-direction (i.e., parallel to the specimen thickness) were referenced to a filtered mean line, thus generating a series of peaks and valleys comprising the surface texture of the foam. The filter was a standard 2RC (resistor-capacitor) type with a nominal cutoff of 2.5 mm [8]. The average roughness, R_a [8], of the surface was defined as the mean of the absolute values of the profile height deviations. Table 3 summarizes values of R_a at the three locations from the sanded specimen 049-21 and from an unsanded specimen of similar polystyrene foam.

Table 3. Average roughness values for foam specimens surfaces

	Average roughness, R_a (µm)	
Location	Sanded	Unsanded
1	16	72
2	20	80
3	16	82

4. Thermal Conductivity Measurement

Thermal conductivity measurements of the expanded polystyrene foam specimens were determined in accordance with ASTM Test Method C 177 [2] using the NIST 1016 mm guarded hot plate apparatus. Section 4 describes the measurement method, experimental design, and specimen selection.

4.1 Guarded-Hot-Plate Method

Figure 8 shows the essential features of the guarded-hot-plate apparatus designed for operation near ambient temperature conditions under operation in the double sided mode. The apparatus is cylindrically symmetric about the axis indicated in Fig. 8. The plates are horizontal and heat flow (Q/2) is vertical (up/down) through the pair of specimens. The NIST 1016 mm diameter guarded hot plate apparatus has been described previously [9-10] and its operation is summarized briefly, here. Two specimens having nearly the same density, size, and thickness are placed on either side of the guarded hot plate and clamped securely by the circular cold plates (F_1 and F_2). Ideally, the guarded hot plate and cold plates provide constant-temperature boundary conditions to the surfaces of the specimens. With proper guarding in the lateral direction, the apparatus is designed to provide one-dimensional heat flow (Q) through the meter area of the specimen pair. A secondary guard is provided by an enclosed chamber that conditions the ambient air surrounding the plates to a temperature near to the mean specimen temperature (i.e., average surface temperatures of the hot and cold plates in contact with the specimens).

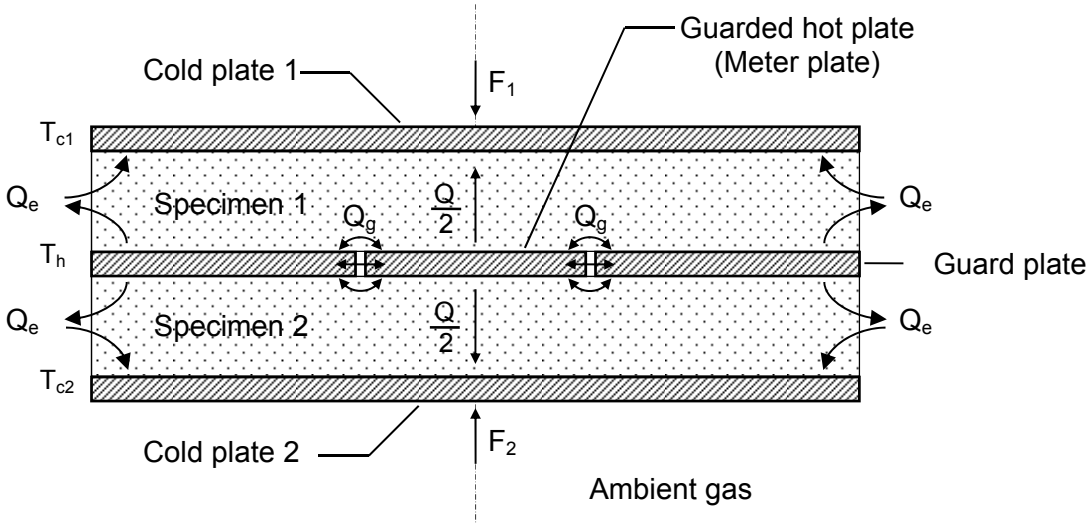

Figure 8. Guarded-hot-plate schematic (not to scale) showing the double-sided mode of operation with vertical heat flow.

Equation (2) is the operational definition [11] for the experimental thermal conductivity[3] of the specimen pair (λ_{exp})

$$\lambda_{exp} = \frac{Q}{A[(\Delta T / L)_1 + (\Delta T / L)_2]} \tag{2}$$

where;

Q = heat flow rate through the meter area of guarded-hot-plate specimen, W;
A = meter area normal to direction of heat flow, m^2;
$\Delta T = T_h - T_c$, temperature difference across specimen, K;
T_h = hot plate temperature, K;
T_c = (average) cold plate temperature, K; and,
L = (in-situ) thickness of guarded-hot-plate specimen, m.

The subscripts 1 and 2 refer to specimen 1 and specimen 2, respectively (Fig. 8). When the temperature differences and the specimen thicknesses are nearly the same, respectively, Eq. (2) reduces to

$$\lambda_{exp} = \frac{Q L_{avg}}{2 A \Delta T_{avg}} \tag{3}$$

In the double-sided mode of operation, values of λ_{exp} were reported at the mean temperature (T_m) of the hot and cold plates, $T_m = (T_h + T_c)/2$.

4.2 Experimental Design and Initial Model

The experimental design for the batch certification of SRM 1453 is based on a model for bulk density and temperature. An initial model for thermal conductivity (λ), bulk density (ρ), and temperature (T) was assumed to be

$$\lambda(\rho, T) = a_0 + a_1\rho + a_2 T + a_3 T^2 + a_4 T^3 \tag{4}$$

Table 4 summarizes a full factorial design having three levels for ρ and five levels for T. This design checks the adequacy of Eq. (4) and also allows checking for the necessity of a quadratic term for ρ, a fourth-order term for T, and/or a cross-product term for ρ and T. Each cell in Table 4 represents one measurement of a different pair of specimens (15 tests in total). The benefit of testing a unique pair of specimens at each combined level of temperature and density is that independent information is obtained at each such level.

[3] The thermal transmission properties of heat insulators determined from standard test methods typically include several mechanisms of heat transfer, including conduction, radiation, and possibly convection. For that reason, some experimentalists will include the adjective "apparent" when describing thermal conductivity of heat insulators. However, for brevity, the term thermal conductivity will be used in this report.

Table 4. Full factorial (3×5) experimental design

	Temperature level (K)				
Density level	281	289	297	305	313
Low	1 obs.[a]⑭	1 obs. ⑦	1 obs. ⑨	1 obs. ⑥	1 obs. ②
Mid	1 obs. ⑤	1 obs. ⑪	1 obs. ①	1 obs. ⑩	1 obs. ⑧
High	1 obs.③	1 obs. ④	1 obs. ⑮	1 obs. ⑫	1 obs. ⑬

[a] observation

The experimental design presented in Table 4 is balanced in the sense that an equivalent amount of information is obtained at each setting of the independent variables. If either extra information had been obtained at some of the settings, or worse, critical information omitted at one setting, the design would be unbalanced and the resulting statistical analysis would suffer. The test sequence, shown as circled numbers (①) in Table 4, was randomized to mitigate systematic effects from other uncontrolled or partially controlled factors that might inadvertently affect the test.

Three nominal levels of ρ were selected to cover the upper and lower limits of the material lot (36 kg/m^3 to 45 kg/m^3). The temperature value of 281 K was effectively fixed by the low limit of the guarded hot plate apparatus. Unfortunately, the limiting value of 281 K is somewhat higher than the low temperature values specified in ASTM Test Method C 1199 [4]. The temperature value of 313 K was selected based on the ASTM material specification for cellular polystyrene thermal insulation [12].

4.3 Test Specimens

A major goal in the selection of the test specimens was to reduce the likelihood of the user extrapolating outside the range of values of bulk density given in the 1453 Certificate. Fifteen pairs of (30) boards, each pair having nearly the same bulk density, were selected from the material lot covering a range from 36 kg/m^3 to 45 kg/m^3. The boards were subsequently cut using a table saw to nominally square dimensions of 657 mm by 657 mm.

The bulk density (ρ_s) for a specimen was determined from Eq. (5):

$$\rho_s = \frac{m_s}{A_s \times L_s} = \frac{m_s}{l_{1s} \times l_{2s} \times L_s} \tag{5}$$

where the subscript s refers to the specimen. The mass (m_s) of the insulation board was measured by a digital weighing balance (32.1 kg range, 0.0001 kg resolution). Dimensional measurements l_{is} (i = 1,2) were determined using a steel rule (0.05 mm resolution). The quantity L_s was averaged from five height gage measurements (0.1 mm resolution) on a granite surface plate.

Table 5 lists the 15 pairs of test specimens and their corresponding bulk density measurements (board and specimen density). The subscripts 1 and 2 refer to two pieces of an individual pair (Fig. 8). The percentage difference ($\Delta\rho_{rel}$) is defined by Eq. (6).

$$\Delta\rho_{rel} = \frac{\left|\rho_2 - \rho_1\right|}{\left(\rho_1 + \rho_2\right)/2} \times 100 \tag{6}$$

Table 5. Bulk density measurements for 30 test specimens

Pair	Density level	ID_1	ID_2	Board density[a] ρ_{1b} (kg/m^3)	Board density[a] ρ_{2b} (kg/m^3)	Board density[a] $\Delta\rho_{b,\,rel}$ (%)	Specimen density[a] ρ_{1s} (kg/m^3)	Specimen density[a] ρ_{2s} (kg/m^3)	Specimen density[a] $\Delta\rho_{s,\,rel}$ (%)
1	Low	023	182	36.62	36.97	0.95	35.93	36.73	2.20
2	Low	168	242	36.98	37.05	0.20	36.77	36.64	0.38
3	Low	073	223	37.32	37.08	0.66	37.69	36.91	2.09
4	Low	059	072	37.53	37.57	0.11	37.58	37.74	0.43
5	Low	019	297	37.67	37.64	0.10	37.95	37.86	0.23
6	Mid	104	156	39.95	39.94	0.03	40.12	39.73	0.96
7	Mid	038	258	39.96	39.97	0.01	40.00	39.58	1.05
8	Mid	126	251	40.01	40.05	0.10	40.14	39.44	1.75
9	Mid	113	210	40.08	40.10	0.04	39.91	39.93	0.04
10	Mid	202	207	40.13	40.11	0.05	39.66	39.90	0.62
11	High	080	120	44.45	44.49	0.09	44.15	43.54	1.38
12	High	042	164	44.59	44.62	0.07	44.26	44.37	0.26
13	High	176	260	44.71	44.78	0.14	44.24	43.76	1.08
14	High	165	238	45.14	44.97	0.37	44.38	44.30	0.18
15	High	239	240	45.16	45.67	1.12	44.44	44.97	1.18

[a] Extra digit included for rounding purposes

4.4 Test Sequence

The bulk density for a specimen pair (i.e., two pieces), ρ_{pair}, was determined from Eq. (7).

$$\rho_{pair} = \left(\rho_{s1} + \rho_{s2}\right)/2 \tag{7}$$

The subscripts 1 and 2 refer to specimen 1 and specimen 2, respectively (Fig. 8). Table 6 summarizes the randomized test sequence for the 15 pairs of expanded polystyrene specimens following the experimental design given in Table 4.

Table 6. Test sequence (fully randomized) for specimen pairs of expanded polystyrene foam

	Test number	Density level	T (K)	ID_1	ID_2	ρ_{1s} (kg/m^3)	ρ_{2s} (kg/m^3)	ρ_{pair} (kg/m^3)
1	1995-018A	Mid	297	104	156	40.1	39.7	39.9
2	1995-019A	Low	313	073	223	37.7	36.9	37.3
3	1995-020A	High	281	080	120	44.1	43.5	43.8
4	1995-021A	High	289	239	240	44.4	45.0	44.7
5	1995-022A	Mid	281	038	258	40.0	39.6	39.8
6	1995-023A	Low	305	059	072	37.6	37.7	37.7
7	1995-024A	Low	289	168	242	36.8	36.6	36.7
8	1995-025A	Mid	313	126	251	40.1	39.4	39.8
9	1995-026A	Low	297	023	182	35.9	36.7	36.3
10	1995-027A	Mid	305	113	210	39.9	39.9	39.9
11	1995-028A	Mid	289	202	207	39.7	39.9	39.8
12	1995-029A	High	305	176	260	44.2	43.8	44.0
13	1995-030A	High	313	042	164	44.3	44.4	44.3
14	1995-031A	Low	281	019	297	37.9	37.9	37.9
15	1995-032A	High	297	165	238	44.4	44.3	44.3

4.5 Test Procedure

The insulation guard material for the thermal conductivity measurements was a fibrous polyester blanket insulation having a diameter of 1016 mm and a square section, 657 mm by 657 mm, removed from the center. This insulation material was selected because of its compressibility and similar thermal conductivity. In separate guarded hot plate tests, the thermal conductivities of 13.3 mm thick specimens of fibrous polyester blanket insulation were determined to be 0.034 W/(m·K), 0.037 W/(m·K), and 0.040 W/(m·K) at T_m of 281 K, 297 K, and 313 K, respectively.

The foam specimens (657 mm by 657 mm) were installed in the guarded-hot-plate apparatus and encircled with the fibrous polyester blanket insulation. The thermal conductivity measurement of each pair of foam specimens was completed in one to two days. During the steady-state test period, data for Q, T_h, and T_c were collected every 2 min. When the plate temperatures were within 0.05 K, or less, of their target temperatures and Q no longer changed monotonically, steady-state data were collected for 4 h and averaged over the time interval.

5. Data Evaluation

Section 5 presents the thermal conductivity measurements (tabular and graphical formats) and uncertainty analyses (for λ_{exp} and ρ) for the foam specimens.

5.1 Data Summary (Tabular Format)

Table 7 summarizes the experimental results – specimen information, input estimates, influencing (secondary) factor estimates, and the output estimate for measured thermal conductivity (λ_{exp}) – for the 15 specimen pairs specified in the experimental design (Table 4). The rows of data in Table 7 are grouped by T_m from 281 K to 313 K and, within each level of T_m, the specimen pair bulk densities (ρ_{pair}) are arranged from lowest to highest value. The columns of data are grouped into the following major sections: specimen material property; input quantities for Eq. (3); secondary quantities; and resultant thermal conductivity (λ_{exp}). The subscripts 1 and 2 designate the top and bottom specimen, respectively, as illustrated in Fig. 8.

Table 7. Thermal conductivity data, sorted by T_m and by ρ_{pair}

		Input quantities for Eq. (3)						Secondary quantities				
T_m	ρ_{pair}	T_h	T_{c1}	T_{c2}	$Q/2$	A	L_{avg}	T_a	p_a	RH	f	λ_{exp} [a]
(K)	(kg/m^3)	(K)	(K)	(K)	(W)	(m^2)	(mm)	(K)	(kPa)	(%)	(kPa)	(W/m·K)
281	37.9	291.15	271.15	271.16	6.177	0.129 79	13.36	281.2	100.8	24	0.75	0.031 81
281	39.8	291.15	271.15	271.16	6.221	0.129 79	13.30	281.2	101.4	23	0.84	0.031 88
281	43.8	291.15	271.15	271.15	6.226	0.129 79	13.25	281.2	101.3	24	1.05	0.031 77
289	36.7	299.15	279.15	279.14	6.346	0.129 84	13.46	289.2	101.4	17	0.69	0.032 89
289	39.8	299.15	279.14	279.15	6.258	0.129 84	13.61	289.2	100.5	18	0.55	0.032 80
289	44.7	299.15	279.15	279.15	6.250	0.129 84	13.52	289.2	101.3	18	0.33	0.032 54
297	36.3	307.15	287.16	287.15	6.505	0.129 89	13.53	297.2	100.5	13	0.98	0.033 90
297	39.9	307.15	287.15	287.15	6.564	0.129 89	13.32	297.2	100.5	14	0.94	0.033 66
297	44.3	307.15	287.15	287.16	6.421	0.129 89	13.53	297.2	100.4	12	1.00	0.033 46
305	37.7	315.15	295.15	295.15	6.741	0.129 93	13.38	305.2	100.3	10	1.38	0.034 70
305	39.9	315.15	295.16	295.14	6.675	0.129 93	13.52	305.2	100.3	10	1.59	0.034 71
305	44.0	315.15	295.15	295.15	6.641	0.129 93	13.48	305.2	100.4	10	1.46	0.034 46
313	37.3	323.15	303.15	303.15	6.955	0.129 98	13.29	313.2	101.2	8	1.65	0.035 56
313	39.8	323.15	303.15	303.15	6.898	0.129 98	13.44	313.2	101.1	8	1.70	0.035 68
313	44.3	323.15	303.15	303.15	6.835	0.129 98	13.41	313.2	100.1	8	1.66	0.035 26

[a] Extra digit included for rounding purposes

For each test, the plate temperatures (T_h, T_{c1}, and T_{c2}) were maintained within 0.01 K, or less, of their respective set-point temperatures such that the specimen ΔT was maintained at 20.0 K. The estimates of $Q/2$ ranged from 6.2 W to 7.0 W for T_m at 281 K and 313 K, respectively. For a fixed value of T_m, the variation of $Q/2$ due to changes in ρ_{pair} was much smaller. The estimates for A have been corrected for thermal expansion effects of the meter-plate (Annex A1.4). The estimates for the in-situ test thickness L were determined by averaging the digital outputs of the eight linear position transducers, four for each cold plate (Annex A1.5). The resultant estimates for λ_{exp} include an extra digit to reduce rounding errors.

During a test, the secondary influence quantities (T_a, p_a, RH, and f) were either controlled or only recorded. The chamber air temperature (T_a) was controlled to be the same temperature as T_m (within 0.1 K, or less). The chamber air pressure (p_a) varied with the site barometric conditions from 100.1 kPa to 101.4 kPa. The chamber RH varied inversely with the chamber dry-bulb air temperature (T_a). The clamping pressure (f) was determined by averaging the loading force (F_1 and F_2 as illustrated in Fig. 8) applied by each cold plate and dividing by the surface area of the specimen surface area in contact with the cold plate. Table 8 provides summary statistics for test quantities in Table 7 that were fixed across all tests.

Table 8. Summary statistics for fixed input quantities and secondary quantities

	ΔT (K)	L_{avg} (mm)	p_a (kPa)	f (kPa)
Mean	20.000	13.43	100.8	1.10
Std. Dev.	0.003	0.11	0.5	0.44

The maximum clamping pressure in Table 7 (f_{max} equal 1.7 kPa) was much less than the mechanical yield point of the polystyrene foam established in Annex 3.

5.2 Uncertainty Budget, λ_{exp}

The measurement uncertainty for λ_{exp} was derived in accordance with current international guidelines [13-14] and described, in detail, in Annex 1. For the multiplicative expression of Eq. (3), the relative combined standard uncertainty in λ_{exp} can be expressed as the relative uncertainties associated with each factor combined in quadrature.

$$u_{c,rel}\left(\lambda_{\exp}\right) = \frac{u_c\left(\lambda_{\exp}\right)}{\lambda_{\exp}} = \sqrt{\left(\frac{u(Q)}{Q}\right)^2 + \left(\frac{u(\Delta T)}{\Delta T}\right)^2 + \left(\frac{u(L)}{L}\right)^2 + \left(\frac{u(A)}{A}\right)^2} \tag{8}$$

The standard uncertainties and input quantities used in Eq. (8) are derived in Annex 1. The maximum combined standard uncertainty for λ_{exp} was determined at T_m of 281 K.

$$u_{c,rel}\left(\lambda_{\exp}\right) = \sqrt{\left(\frac{0.0068}{6.169}\right)^2 + \left(\frac{0.077}{20.000}\right)^2 + \left(\frac{0.061}{13.31}\right)^2 + \left(\frac{0.000023}{0.12979}\right)^2} \tag{9}$$

$$u_{c,rel}\left(\lambda_{\exp}\right) = \sqrt{(0.00110)^2 + (0.00385)^2 + (0.00458)^2 + (0.00018)^2} = 0.0061 \tag{10}$$

$$U_{rel}\left(\lambda_{\exp}\right) = 2\,u_{c,rel}\left(\lambda_{\exp}\right) = 0.012 \tag{11}$$

Expressed as a percent (× 100), U_{rel} is equal to 1.2 %.

The relative contribution for the first term in Eq. (10) is 3.3 %; for the second, 40.0 %; for the third, 56.6 %; and, for the fourth, 0.1 %. The major contributory uncertainties for SRM 1453 are due to the empirical determinations for specimen thickness (L_{avg}) and temperature difference (ΔT).

5.3 Data Screening (Graphical Analysis)

Values of λ_{exp} from Table 7 are plotted in Figs. 9a and 9b as a function of the model input variables ρ and T, respectively. Figure 9a plots the individual data points as filled circle symbols corresponding to T levels of 281 K, 289 K, 297 K, 305 K, and 313 K. The error bars represent expanded uncertainties of 1.2 % (Sec. 5.2). Figure 7b plots the individual data points as filled circle, square, and triangle symbols (without error bars for clarity) corresponding to the three levels selected for bulk density.

The data in Fig. 9 strongly suggests that, in the range of ρ and T covered for the 300 boards, comprising the current SRM:

1) λ_{exp} is slightly sensitive to ρ; and,
2) the dependency of λ_{exp} on T is linear.

The first assertion is supported by the linear least squares fits to the 3-point negatively-sloped horizontal profiles visible in Fig. 9a. For the bulk density range of 37.4 kg/m^3 to 45.8 kg/m^3, the change in thermal conductivity with respect to bulk density was quite small and, for the most part, decreased as bulk density increased (Fig. 9a). As discussed in Sec. 5.4, the small dependency on ρ required a correction for the metered section bulk density. The second assertion is supported by the data in Fig. 9b that shows, over a range of 281 K to 313 K, λ_{exp} increased linearly by about 12 % (from 0.0316 W/(m·K) to 0.0354 W/(m·K)).

5.4 Correction for Metered Section Bulk Density

The data in Fig. 9a indicate that λ_{exp} is slightly dependent on ρ. To determine the effect of the metered section density, the insulation cylinder above and below the meter plate (Fig. 8) was cut for mass determination (m_m). The metered section bulk density [2] is defined in Eq. (12) as

$$\rho_m = \frac{m_m}{A_m \times L_m} = \frac{m_m}{\left(\pi r^2\right) \times L_m} = \frac{4 m_m}{\left(\pi d^2\right) \times L_m} \tag{12}$$

where the subscript m refers to the metered section (in this case, a right-angle cylinder); and, r and d are the radius and diameter, respectively, of the round cylinder.

In order to preserve particular specimens of interest for future measurements, a specific subset of only eight specimens (four pairs) was selected for cutting. Table 9, which follows the same format as the experimental design presented in Table 4, summarizes the specimen pairs that were selected for the determination of the metered section bulk density.

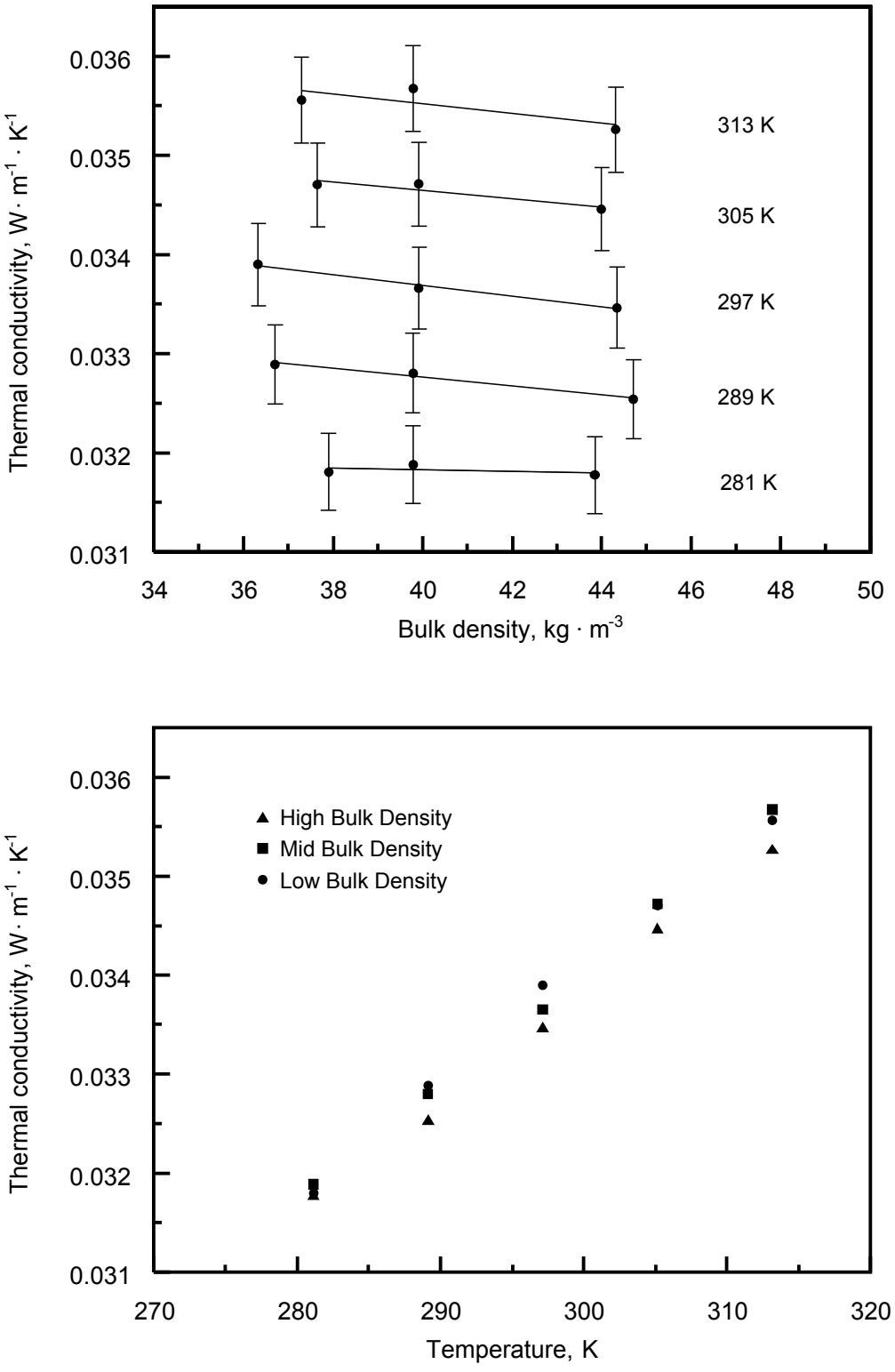

Figure 9. SRM 1453 a) Graphical analysis of thermal conductivity versus bulk density (uncorrected). Error bars represent expanded uncertainties of 1.2 %. b) Graphical analysis of thermal conductivity (without error bars for clarity) versus temperature.

Table 9. Specimens selected for metered section bulk density measurements (see Table 4)

	Temperature level (K)				
Density level	281	289	297	305	313
Low	---	168, 242	---	059, 072	---
Mid	---	---	---	---	---
High	---	239, 240	---	176, 260	---

Using a jigsaw, 406 mm diameter cylinders were cut from the center of each of the eight specimens and weighed. The mass (m_m) of the metered section was measured by a digital weighing balance (32.1 kg range, 0.0001 kg resolution). Dimensional measurements for the diameter d were determined using a steel rule (0.05 mm resolution). The quantity L_m was averaged from five height gage measurements (0.1 mm resolution) of the metering section placed on a granite surface plate.

For a specimen pair, Eq. (13) defines the correction for the metered section bulk density:

$$\rho_{pair,corr} = \rho_{pair} + \overline{\rho}_{corr} \tag{13}$$

Substituting Eq. (7) for the first term in Eq. (13) and expanding the second term yields:

$$\rho_{pair,corr} = \frac{\rho_{s1} + \rho_{s2}}{2} + \frac{1}{8}\sum_{i=1}^{8}\left(\rho_m - \rho_s\right)_i \tag{14}$$

Values for ρ_s, ρ_m, and $\rho_m - \rho_s$ were determined for the eight specimens and are summarized in Table 10. The differences ($\rho_m - \rho_s$) range from 0.1 kg/m^3 to 2.1 kg/m^3. As observed in Fig. 6, and confirmed in Table 10, the bulk-density variation within a board was generally higher near the center and lower near the edges.

Table 10. Comparison of specimen and meter area bulk densities

ID	Density level	ρ_s[a] (kg/m^3)	ρ_m[a] (kg/m^3)	$(\rho_m - \rho_s)$[a] (kg/m^3)
242	Low	36.64	38.49	1.85
072	Low	37.74	38.68	0.94
059	Low	37.58	38.61	1.03
168	Low	36.77	38.83	2.06
176	High	44.24	44.92	0.68
260	High	43.76	45.06	1.30
239	High	44.44	44.84	0.40
240	High	44.97	45.06	0.09
			Mean	1.05
			Std. dev.	0.67

[a] Extra digit included for rounding purposes

From Table 10, the mean of the differences ($\overline{\rho}_{corr}$) and the standard deviation (s) were 1.05 kg/m^3 and 0.67 kg/m^3, respectively. A 95 % confidence interval for the "true" density difference was determined from Eq. (15):

$$\overline{\rho}_{corr} \pm t_{\alpha/2,\mathrm{DoF}} \frac{s}{\sqrt{n}} \tag{15}$$

where (Student's) t for 95 % and 7 degrees of freedom (DoF) is 2.36, and n is the number of measurements (8). The corresponding interval was 1.05 kg/m^3 ± 0.56 kg/m^3 which does not contain zero. Therefore, the difference in densities for the meter area and the entire specimen was statistically significant and a value of 1.05 kg/m^3 was added using Eq. (13) to the specimen pair bulk densities (ρ_{pair}) of Table 7 for the regression analyses (Sec. 6) to account for the metered section bulk density.

5.5 Standard Uncertainty for the Metered Section Bulk Density Correction

The measurement uncertainties for ρ_s, ρ_m, and $\rho_{pair,corr}$ were derived in accordance with current international guidelines [13-14] and described, in detail, in Annex 2. The standard uncertainties for these quantities are as follows:

- $u_c(\rho_s)$ is 0.18 kg/m^3 (from Eq. (A2-5));
- $u_c(\rho_m)$ is 0.27 kg/m^3 (from Eq. (A2-9)); and,
- $u_c(\rho_{pair,corr})$ is 0.42 kg/m^3 (from Eq. (A2-11)).

6. Regression Analysis

Section 6 describes the regression analysis of the data. There are two goals for this analysis:

1) to estimate a predictive relationship between λ and the predictors ρ and T; and,
2) to quantify the uncertainty in predictions from this estimated relationship.

In the first stage of the analysis, a model is selected by considering all subsets of the regression terms $\{\rho_{pair,corr}, T_m, T_m^2, T_m^3\}$ (with response λ_{exp}), where the Bayesian information criterion (BIC) [15] is used for comparison. In the second stage, the final estimate of the predictive relationship and the expanded uncertainty (U) for predictions from that estimated relationship are calculated using a measurement error model [16] and the Bayesian inference paradigm [17].

6.1 Model Selection

The experiment was designed so that each of the factors, $\rho_{pair,corr}$, T_m, T_m^2, and T_m^3 could be included as predictors in a multiple regression model (with response λ_{exp}). To choose a model, the BIC for all 16 subsets of regression terms are calculated. The BIC can be thought of as applying the parsimony principle to model selection. That is, it seeks the simplest model that provides a good description of the observed data. More directly, the BIC is the sum of two terms. The first term describes the fit of the model to the observed data, and the second term involves a positive penalty for the number of parameters (regression coefficients) in the model. Models providing a good fit to the data have small first terms, and models with more parameters receive a larger penalty. Since more parameters typically lead to a better fit, these two terms fight against one another, and we select the model with the smallest BIC. The BIC values for all 16 models under consideration are given in Table 11. From Table 11, it can be seen that the model with $\rho_{pair,corr}$ and T_m is best (i.e., Rank 1).

Table 11. BIC values for all models under consideration.

Model	BIC	Rank
$\rho_{pair,corr}$, T_m	-82.13	1
$\rho_{pair,corr}$, T_m^2	-80.25	2
$\rho_{pair,corr}$, T_m, T_m^2	-79.52	3
$\rho_{pair,corr}$, T_m, T_m^3	-79.52	3
$\rho_{pair,corr}$, T_m^2, T_m^3	-79.52	3
$\rho_{pair,corr}$, T_m, T_m^2, T_m^3	-77.34	6
$\rho_{pair,corr}$, T_m^3	-76.71	7
T_m	-63.85	8
T_m^2	-63.28.	9
T_m^3	-62.14	10
T_m, T_m^3	-61.20	11
T_m^2 T_m^3	-61.20	11
T_m, T_m^2	-61.19	13
T_m, T_m^2, T_m^3	-58.59	14
Intercept only	0.00	15
$\rho_{pair,corr}$	2.58	16

To verify that the model with $\rho_{pair,corr}$ and T_m actually provides a good fit to the data, plots of the deviations (also known as residuals) from a least squares fit are examined. In Fig. 10, a normal quantile-quantile plot of the deviations as well as plots of the deviations against $\rho_{pair,corr}$, T_m, and the predicted values of λ are shown.

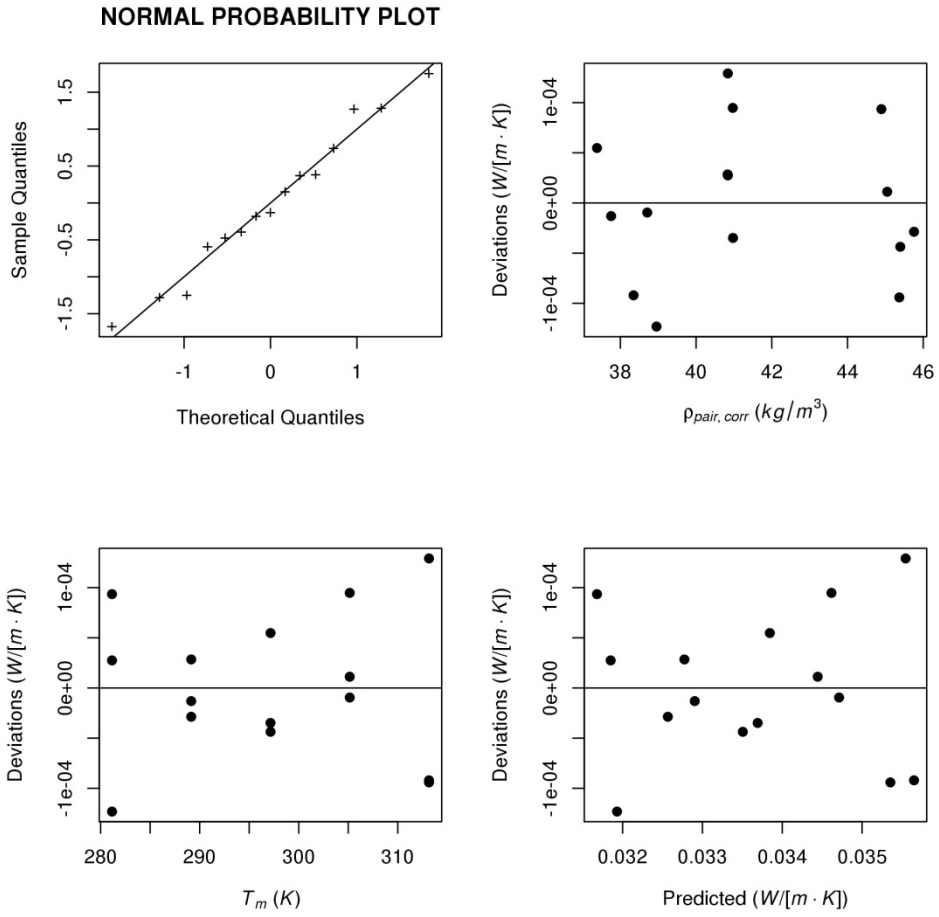

Figure 10. Plots of deviations (also known as residuals) for assessing the model fit.

The normal quantile-quantile plot indicates no problems as the points follow a reasonably straight line. The plots of the deviations versus $\rho_{pair,corr}$, T_m, and the predicted values of λ also indicate no problems since the deviations form a symmetric horizontal band around zero.

6.2 Estimation and Uncertainty

The final estimation of the predictive relationship as well as the uncertainty quantification in predictions from this relationship is carried out using a measurement error model [16] and the Bayesian inference paradigm [17]. A detailed description of the analysis is found in Annex 4. The final equation and expanded uncertainty on the certificate is

$$\lambda = 0.00111 - 0.000\,042\,4\rho + 0.000\,115T \quad \pm 1.5\,\%\,(k = 2). \tag{16}$$

The uncertainty represents an interval in which a new hypothetical NIST measurement of thermal conductivity will lie with at least 95% posterior predictive probability. In Sec. 5.2, Eq. (11) the expanded uncertainty for λ_{exp} is 1.2 %. The additional uncertainty in predictions from the above equation comes from various other sources. For example, the predictive relationship, while quite good, does not perfectly predict the λ_{exp}.

7. Certification

Section 7 presents summary information on the properties of interest, values and uncertainty, and instructions for use for Standard Reference Material 1453. This information is intended to provide supplementary documentation for the 1453 Certificate.

7.1 Properties of Interest

Standard Reference Material 1453 is an expanded polystyrene foam board certified for thermal conductivity, λ. Each SRM unit consists of a rectangular panel of expanded polystyrene beads molded into a semi-rigid board. The nominal dimensions of a unit are 931 mm by 657 mm by 13.2 mm (Table 1) and the bulk density ranges from 37 kg/m^3 to 46 kg/m^3 (Table 6).

7.2 Values and Uncertainties

Each unit of SRM 1453 is batch certified for thermal conductivity with Eq. (17):

$$\lambda = 0.00111 - 0.000\,042\,4\,\rho + 0.000\,115\,T_m \quad \pm 1.5\,\%\ (k = 2) \tag{17}$$

where λ is the predicted thermal conductivity (W/(m·K)) and T_m is the mean specimen temperature (K). The test temperature difference across the specimen (ΔT) was 20 K (Table 8). Equation (17) is only certified to be valid over the bulk density range from 37 kg/m^3 to 46 kg/m^3 and temperature range from 281 K to 313 K. The expanded uncertainty for λ values from Eq. (17) is 1.5 % with a coverage factor of approximately $k = 2$.

7.3 Instructions for Use

Standard Reference Material 1453 is intended for use as part of a calibration transfer standard for the thermal evaluation of fenestration systems using a hot box test method. The SRM is also intended for use as a proven check for the guarded-hot-plate apparatus (or other absolute thermal conductivity apparatus) and for calibration of a heat-flow-meter apparatus over the temperature range of 281 K to 310 K. NIST cannot exclude the use of SRM 1453 for other purposes, but the user is cautioned that other purposes are not sanctioned by the 1453 Certificate.

7.3.1 Storage

For protection and identification, it is recommended that the reference material be stored in the original packaging in a clean, dry environment at temperatures between 15 °C and 30 °C.

7.3.2 Preparation and Conditioning before Measurement

Prior to the thermal conductivity measurement, the reference material should be conditioned in laboratory conditions of 20 ° C to 25 °C and from 40 % RH to 65 % RH until the mass of the unit is stable (i.e., two successive measurements within 24 h vary by less than 1 %). It should be noted, however, that polystyrene foam is insensitive to changes in humidity as described in Annex 5.

7.3.3 Thermal Conductivity Measurement

Thermal conductivity measurements should be conducted in accordance with the appropriate ASTM Test Method C 177 [2], C 518 [3], or other comparable standard. Measurement as part of a fenestration test should be conducted in accordance with ASTM Test Method C 1199 [4] or other similar standard.

7.3.4 Guidelines and Precautions

The following guidelines and precautions are provided for the user.

3) *Stacking*: Certified values of thermal conductivity are valid for a single unit, and are invalid for stacked units. The thermal conductivity of polystyrene foam dramatically increases with specimen thickness due to the increased transmission of long-wave thermal radiation in thicker specimens [18-19].
4) *Slicing*: Certified values of thermal conductivity are invalid for a unit where the thickness of the material has been modified by slicing.
5) *Cutting*: It is possible to cut the reference material unit into smaller pieces. It is imperative to verify that bulk density of each piece is within the certified range of bulk density (Sec. 7.1).
6) *Upper Temperature Limit*: The upper temperature for SRM 1453 is limited to the softening point of the polystyrene polymer which is 347 K (74 °C) [12]. It should be noted that oven drying, as opposed to desiccant drying, can remove other volatiles and potentially affect chemical or physical properties of the material.
7) *Lower Temperature Limit*: A lower temperature limit for SRM 1453 has not been established but, in principle, there is no known lower limit.
8) *Atmospheric Pressure*: The effect due to changes in ambient atmospheric pressure is negligible for this material.
9) *Clamping Pressure*: For thermal testing, the specimens must be in firm contact with the apparatus plates. However, do not compress the material more than 0.34 mm (2.5 %) of its original thickness. The compressive resistance of expanded polystyrene foam is described in Annex 3.
10) General precautions for handling polystyrene foam are described in Annex 6.

Acknowledgments

The original 1995 certification of SRM 1453 was accomplished with the assistance of the following individuals. Nancy Trahey and Robert Gettings provided support through the Standard Reference Materials Program. NIST Statistician, Dr. E. S. Lagergren provided the initial guidance in the experimental design and data analysis. The surfaces of the foam boards were prepared by R. L. Baumgardner of Rollin, Inc. Micrographs of the foam were filmed by P. E. Stutzman and compressive resistance measurements provided by J. Seiler and Dr. W. J. Rossiter. The surface roughness measurements were provided by C. K. Rymes and J. F. Song. Sorption isotherm measurements were supervised by D. Burch and C. Saunders assisted with the density measurements of the 300 foam boards.

References

[1] J. K. Taylor, "Standard Reference Materials, Handbook for SRM Users," *NIST Special Publication 260-100*, Natl. Inst. Stand. Technol., February 1993.

[2] ASTM, "C 177 Standard Test Method for Steady-State Heat Flux Measurements and Thermal Transmission Properties by Means of the Guarded Hot Plate Apparatus," *Annual Book of ASTM Standards, Vol. 04.06*.

[3] ASTM, "C 518 Standard Test Method for Steady-State Thermal Transmission Properties by Means of the Heat Flow Meter Apparatus," *Annual Book of ASTM Standards, Vol. 04.06*.

[4] ASTM, "C 1199 Standard Test Method for Measuring the Steady-State Thermal Transmittance of Fenestration Systems Using Hot Box Methods," *Annual Book of ASTM Standards, Vol. 04.06*.

[5] "Energy Policy Act of 1992," Act of October 24, 1992, Public Law 102-486, 102nd Congress.

[6] R. P. Bowen and K. R. Solvason, "A Calorimeter for Determining Heat Transmission Characteristics of Windows," *Thermal Insulation: Materials and Systems, ASTM STP 922*, F. J. Powell and S. L. Matthews, Eds., American Society for Testing and Materials, Philadelphia (1987) 567-581.

[7] W. P. Goss, H. A. Elmahdy and R. P. Bowen, "Calibration Transfer Standards for Fenestration Systems," *In-Situ Heat Flux Measurements in Buildings: Applications and Interpretations of Results, CRREL Special Report 91-3*, S. N. Flanders, Ed., (1991) 251-260.

[8] ASME, "Surface Texture: Surface Roughness, Waviness, and Lay," *B46.1-1995*, ISBN**:** 0791823563.

[9] F. J. Powell and B. G. Rennex, "The NBS Line-Heat-Source Guarded Hot Plate for Thick Materials," *Thermal Performance of the Exterior Envelopes of Buildings - II, ASHRAE SP 38* (1983) 657-672.

[10] R. R. Zarr and M. H. Hahn. "Line Heat Source Guarded Hot Plate Apparatus," *Adjunct ASTM Practice C 1043*, PCN: 12-310430-61.

[11] ASTM, "C 1045 Standard Practice for Calculating Thermal Transmission Properties Under Steady-State Conditions," *Annual Book of ASTM Standards, Vol. 04.06*.

[12] ASTM, "C 578 Standard Specification for Rigid, Cellular Polystyrene Thermal Insulation," *Annual Book of ASTM Standards, Vol. 04.06*.

[13] B. N. Taylor and C. E. Kuyatt, "Guidelines for Evaluating and Expressing the Uncertainty of NIST Measurement Results," *NIST Technical Note 1297*, Natl. Inst. Stand. Technol. 1994.

[14] ISO, *Guide to the Expression of Uncertainty in Measurement*, International Organization for Standardization, Geneva, Switzerland, 1993.

[15] G. Schwarz, "Estimating the Dimension of a Model," *The Annals of Statistics*, 6, 461-464 (1978).

[16] W. Fuller, Measurement Error Models, John Wiley & Sons, Inc., New York (1985).

[17] A. Gelman, J. B. Carlin, H. S. Stern, and D. B. Rubin, Bayesian Data Analysis, 2nd Ed., Chapman & Hall/CRC, Boca Raton, Florida (2004).

[18] J. R. Booth and J. T. Grimes, "The Determination of Radiation k-Factor for Foam Structures Using HFM Apparatus," *Thermal Conductivity 22*, Technomic: Lancaster, Pennsylvania (1994) 783-793.

[19] T. T. Jones, "The Effect of Thickness and Temperature on Heat Transfer Through Foamed Plastics," *Plastics and Polymers*, February, 33-39 (1972).

[20] Y. S. Touloukian, R. K. Kirby, R. E. Taylor, and P. D. Desai, *Thermophysical Properties of Matter, The TPRC Data Series, Volume 12: Thermal Expansion: Metallic Elements and Alloys*. IFI/Plenum, New York (1977) pp. 1028-1033.

[21] R. K. Burdick, Confidence Intervals on Variance Components, 1992, p. 66.

[22] R. J. Roark, Formulas for Stress and Strain, 4th Ed. McGraw-Hill Inc., New York (1965) p. 219.

[23] B. G. Rennex, "Error Analysis for the National Bureau of Standards 1016 mm Guarded Hot Plate," *NBSIR 83-2674*, Natl. Inst. Stand. Technol., February 1983 (reprinted in *Journal of Thermal Insulation*, 7, 18-51 (July 1983)).

[24] M. H. Hahn, H. E. Robinson, and D. R. Flynn, "Robinson Line-Heat-Source Guarded Hot Plate Apparatus," *Heat Transmission Measurements in Thermal Insulations*, *ASTM STP 544* (1974) pp. 167-192.

[25] ASTM, "C 165 Standard Test Method for Measuring Compressive Properties of Thermal Insulation," *Annual Book of ASTM Standards, Vol. 04.06*.

[26] A. Gelman, "Prior distributions for variance parameters in hierarchical models," *Bayesian Analysis*, 1, 515-533 (2006).

[27] D. Lunn, D. Spiegelhalter, A. Thomas, and N. Best, "The BUGS project: Evolution, critique, and future directions," *Statistics in Medicine*, 28, 3049-3067 (2009).

[28] R Development Core Team, R: A language and environment for statistical computing, R Foundation for Statistical Computing, Vienna, Austria (2012); http://www.R-project.org [Accessed (Aug 2012)].

[29] S. Mehta, S. S. Biederman, and S. Shivkumar, "Thermal Degradation of Foamed Polystyrene," *Journal of Materials Science,* 30, 2944-2949 (1995).

Annex 1

Annex 1 - Uncertainty Analysis for Thermal Conductivity (λ)

A1.1 Background

In 1992, NIST officially adopted a new policy [13] for the expression of measurement uncertainty consistent with international practices set forth in the ISO *Guide to the Expression of Uncertainty in Measurement* [14], also known as the "GUM." This policy provides a uniform approach at NIST to uncertainty analysis and is summarized briefly below.

In many cases, a measurand, Y, is not determined directly from a measurement, but rather mathematically from a function of N other *independent* quantities X_i:

$$Y = f\left(X_1, X_2, ..., X_N\right) \tag{A1-1}$$

The output estimate of Y, denoted as y, is obtained using input estimates x_i for the values of the N independent quantities X_i:

$$y = f\left(x_1, x_2, ..., x_N\right) \tag{A1-2}$$

The combined standard uncertainty of y, $u_c(y)$, is the positive square root of the combined variance, $u_c^2(y)$; where

$$u_c^2(y) \approx \sum_{i=1}^{N}\left(\frac{\partial f}{\partial x_i}\right)^2 u^2(x_i) = \sum_{i=1}^{N} c_i^2\, u^2(x_i) \tag{A1-3}$$

Equation (A1-3) is commonly referred to as the "law of propagation of uncertainty". The partial derivatives are known as sensitivity coefficients (c_i) and are equal to $\partial f / \partial X_i$ evaluated at $X_i = x_i$. The corresponding term, $u(x_i)$, is the standard uncertainty associated with the input estimate x_i.

Each standard uncertainty, $u(x_i)$, is evaluated as either a Type A or Type B methods. Standard uncertainties are denoted as Type A if they are evaluated by statistical means. Standard uncertainties that cannot be determined directly from the experiment at hand and are evaluated by scientific judgement including information from (previous) measurement data from another experiment, experience, a calibration certificate, manufacturer specification, among others. [13-14]. Standard uncertainties evaluated using these types of analysis methods are denoted Type B. Categorizing the evaluation of uncertainties as Type A or Type B is simply a matter of convenience, since both are based on probability distributions[4] and combined equivalently in Eq. (A-3). An example of a Type A evaluation is provided below. Examples of Type B evaluations are provided in Refs. [13-14]. It should be noted that the designations "A" and "B" apply to the two methods of evaluation, not the type of error.

[4] The probability distribution for a Type B evaluation, as opposed to a Type A evaluation, is assumed based on the experimenter's judgment.

Annex 1

As an example of a Type A evaluation, consider an input quantity X_i determined from n independent observations obtained under the same conditions (i.e., repeated observations). In this case, the input estimate x_i is the sample mean determined from:

$$x_i = \bar{X}_i = \frac{1}{n}\sum_{k=1}^{n} X_{i,k} \tag{A1-4}$$

The standard uncertainty, $u(x_i)$ associated with x_i is the estimated standard deviation of the sample mean:

$$u(x_i) = s(\bar{X}_i) = \frac{s}{\sqrt{n}} \tag{A1-5}$$

When an uncertainty bound that provides an interval that will contain the true value of the measurand with high probability is required (similar to a confidence interval used for decision making, for example), an expanded uncertainty, U, is obtained by multiplying the combined standard uncertainty, $u_c(y)$, by a coverage factor, k:

$$U = k\,u_c(y) = k\sqrt{\sum c_i^2 u^2(x_i)_A + \sum c_i^2 u^2(x_i)_B} \tag{A1-6}$$

The value of k is chosen based on the desired level of confidence to be associated with the interval defined by U and typically ranges from 2 to 3. Interpretation of the coverage factor requires a word of caution. The term "confidence interval" has a specific definition in statistics and is only applicable to intervals based on u_c when certain conditions are satisfied, including that *all* components of u_c be obtained from Type A evaluations. Under these circumstances, assuming the inputs with the most significant uncertainties are based on relatively large sample sizes, a coverage factor of $k = 2$ defines an interval having a level of confidence of about 95 % and $k = 3$ defines an interval having a level of confidence greater than 99 %. At NIST, the value of the coverage factor is $k = 2$, by convention [13].

A1.2 Uncertainty for λ_{exp}

Referring to Eq. (3) in Sec. 4.1, the standard uncertainty for λ_{exp} was evaluated based on the standard uncertainties for the specimen heat flow (Q), meter area (A), *in-situ* thickness (L), and specimen temperature difference (ΔT). These individual standard uncertainties were evaluated by either statistical methods (Type A), other means (Type B), or both, and are discussed below.

A1.3 Specimen Heat Flow (Q)

Under normal operation (Fig. 8), the guard plate and ambient air temperature were maintained such that lateral heat losses (Q_g and Q_e) were reduced to negligible proportions. Under these circumstances, the specimen heat flow (Q) was determined by simply measuring the direct current (DC) electrical power provided to the meter area (Q_m) of the guarded hot plate. The electrical circuit for the measurement consisted of a standard resistor, nominally 0.1 Ω, in series with the electrical heater of the meter area as illustrated in Fig. A1.

Annex 1

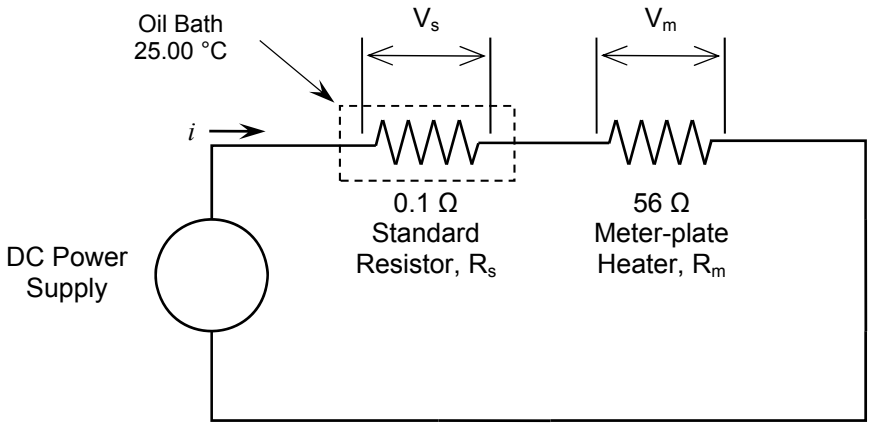

Figure A1. Electrical schematic for meter-plate power measurement.

The corresponding equation for the power input to the meter area is:

$$Q_m = i V_m = \left(\frac{V_s}{R_s} \right) V_m \tag{A1-7}$$

where i is the current (V_s / R_s) through the circuit and V_m is the voltage drop measured across the electrical leads to the meter plate.

A1.3.1 Uncertainty for Power Measurement (Q_m)

The Type A standard uncertainty for Q_m was determined by pooling the standard deviations for each guarded hot plate test. The uncertainty estimates for $u(Q_m)_A$ are tabulated at the end of this section.

The Type B standard uncertainty for Q_m was determined by application of Eq. (A1-3) to Eq. (A1-7) which yields

$$u_c(Q_m)_B = \sqrt{c_{V_s}^2 \, u^2(V_s)^2 + c_{R_s}^2 \, u^2(R_s)^2 + c_{V_m}^2 \, u^2(V_m)^2} \tag{A1-8}$$

with

$$c_{V_s} = \frac{\partial Q_m}{\partial V_s} = \frac{V_m}{R_s}$$

$$c_{R_s} = \frac{\partial Q_m}{\partial R_s} = -\frac{V_s}{R_s^2} V_m$$

$$c_{V_m} = \frac{\partial Q_m}{\partial V_m} = \frac{V_s}{R_s}$$

Annex 1

The input values for R_s and $u(R_s)$ in Eq. (A1-8) were equal to 0.100071 Ω and 0.000001 Ω (k = 1), respectively. The standard uncertainties for V_s and V_m were determined from Eq. (A1-9).

$$u(V) = \frac{a}{\sqrt{3}} \tag{A1-9}$$

The Type B standard uncertainties for V_s and V_m (Fig. A1) were assumed to have a uniform distribution in the interval $\pm a$; where $\pm a$ was determined from the manufacturer specification for the integrating digital voltmeter (DVM). The interval half-widths, a, for V_s and V_m (300 mV and 30 V ranges, respectively) were based on the 1 year manufacturer specification for the integrating voltmeter and were computed from Eqs. (A1-10a) and (A1-10b), respectively, where *reading* is in volts.

$$V_s:\ a = 0.00008 \times reading\ +\ 8\ \mu V\ +\ 0.0001 \times reading \tag{A1-10a}$$

$$V_m:\ a = 0.00008 \times reading\ +\ 300\ \mu V\ +\ 0.0001 \times reading \tag{A1-10b}$$

Table A1.1 summarizes the standard uncertainty components for $u(Q_m)$ for T_m at 281 K, 297 K, and 313 K. The Type B evaluations in Table A1.1 are about 4 times greater than the Type A evaluations. There is a slight increase in the uncertainty with T_m.

Table A1.1. Summary of standard uncertainty components for $u(Q_m)$

T_m (K)	$u(Q_m)_A$ (W)	V_s (V)	$u(V_s)$ (V)	V_m (V)	$u(V_m)$ (V)	$u(Q_m)_B$ (W)
281	0.000 67	0.047	0.000 009 5	26.3	0.0029	0.0028
297	0.000 72	0.048	0.000 009 6	27.0	0.0030	0.0030
313	0.000 72	0.049	0.000 009 7	27.8	0.0031	0.0031

A1.3.2 Guard Imbalance (Q_g)

The terms Q_g and Q_e (Fig. 8) represent both the lateral heat loss at the guard gap between the meter plate and guard plate (Q_g) and the heat loss at the edges of the specimens (Q_e). These effects were quite small (approximately zero) for the 15 guarded hot plate tests (Sec. 4.1) because guarding at the gap and edges of the specimen reduced the lateral heat flows Q_g and Q_e to negligible proportions (Fig. 8). An imbalance condition is defined when a significant temperature difference develops either across the gap (V_g) or at the edge of the specimens ($T_a - T_m$). The first parameter, V_g, is the voltage output from an 8-junction Type-E thermopile across the gap. The second parameter, $T_a - T_m$, is the temperature difference between the ambient air and mean temperature.

Table A1.2 summarizes the imbalance settings for two treatments (V_g and $T_a - T_m$) for five test conditions. The last row in Table A1.2 is a center point where V_g and $T_a - T_m$ were both set to zero; that is, under normal operating conditions for negligible heat flows

at the guard gap and specimen edges. This experimental design checks previous results and any interaction between the independent factors.

Table A1.2. Nominal settings for imbalance study

Index	V_g (μV)	$T_a - T_m$ (K)
1	–50	–5
2	+50	–5
3	–50	+5
4	+50	+5
5	0	0

The test sequence shown in Table A1.2 was randomized for each level of T_m at 281 K, 297 K, and 313 K (5+5+5 = 15 tests). The tests were conducted with one pair of specimens of expanded polystyrene boards (202, 207) installed in the guarded-hot-plate apparatus and encircled with fibrous polyester. During each test, the steady-state power input to the meter plate (Q_m) was recorded and averaged for the test. The imbalance effect, ΔQ, was defined as:

$$\Delta Q = Q_m - Q_{m0} \tag{A1-11}$$

where Q_{m0} was the power input to the meter plate for the gap and edge temperatures thermally balanced, i.e., at the center point where V_g and $T_a - T_m$ were both set to zero. Table A1.3 summarizes the test results from the imbalance study at T_m of 281 K, 297 K, and 313 K.

Table A1.3. Test results for imbalance study (Yates order)

Index	T_m (K)	ΔT (K)	Q_m (W)	y $(Q_m - Q_{m0})$ (W)	x_1 $(V_g - V_{g0})$ (μV)	x_2 $[(T_a - T_m) - (T_a - T_m)_0]$ (K)
1	281	20.00	11.9901	-0.1458	-50.01	-4.97
2	281	20.00	12.2175	0.0816	49.96	-4.99
3	281	20.00	12.0512	-0.0847	-50.00	5.00
4	281	20.00	12.2727	0.1368	50.00	5.00
5	281	20.00	12.1359	0.	0.	0.
1	297	20.00	12.7124	-0.1240	-50.00	-5.00
2	297	20.00	12.9375	0.1011	49.96	-5.00
3	297	20.00	12.7330	-0.1034	-50.03	5.01
4	297	20.00	12.9549	0.1185	49.97	5.00
5	297	20.00	12.8364	0.	0.	0.
1	313	20.00	13.3952	-0.1260	-49.99	-4.99
2	313	20.00	13.6351	0.1139	50.00	-4.99
3	313	20.00	13.4123	-0.1089	-49.97	5.01
4	313	20.00	13.6449	0.1237	50.	5.01
5	313	20.00	13.5212	0.	0.	0.

Annex 1

The response variable (y) and input variables (x_1, x_2) were normalized with respect to the balance point. Negative values for x_1 indicate that the guard plate is warmer than the meter plate (Fig. 8). Conversely, positive values for x_1 indicate that the guard plate is cooler than the meter plate.

The data in Table A1.3 were fit to the model given in Eq. (A1-10). The presence of an offset coefficient b_0 was initially considered but, because the term is predicted to be nearly zero from theory, the term was not included.

$$y = \Delta Q = b_1 x_1 + b_2 x_2 \tag{A1-12a}$$

$$y = b_1 \left(V_g - V_{g0} \right) + b_2 \left[\left(T_a - T_m \right) - \left(T_a - T_m \right)_0 \right] \tag{A1-12b}$$

Table A1.4 summarizes the parameter estimates and approximate standard deviations from multiple variable linear regression for coefficients b_1 and b_2 at T_m of 281 K, 297 K, and 313 K.

Table A1.4. Parameter estimates and standard deviations for b_1 and b_2 in Eq. (A1-12)

T_m (K)	b_1 (W/μV)	$s(b_1)$ (W/μV)	b_2 (W/K)	$s(b_2)$ (W/K)	Residual SD (W)
281	2.245×10^{-3}	3.94×10^{-5}	5.819×10^{-3}	3.95×10^{-4}	0.0039
297	2.236×10^{-3}	2.39×10^{-5}	1.902×10^{-3}	2.39×10^{-4}	0.0024
313	2.363×10^{-3}	2.23×10^{-5}	1.339×10^{-3}	2.23×10^{-4}	0.0022

Application of Eq. (A1-3) to Eq. (A1-12a) yields

$$u_c\left(y\right) = u_c\left(\Delta Q\right) = \sqrt{c_{b_1}^2 u^2\left(b_1\right) + c_{x_1}^2 u^2\left(x_1\right) + c_{b_2}^2 u^2\left(b_2\right) + c_{x_2}^2 u^2\left(x_2\right)} \tag{A1-13}$$

with

$$c_{b_i} = \frac{\partial\left(\Delta Q\right)}{\partial b_i} = x_i$$

$$c_{x_i} = \frac{\partial\left(\Delta Q\right)}{\partial x_i} = b_i$$

Note that no term for the correlation between b_1 and b_2 is required in Eq. (A1-13) because the experiment design used in the assessment of the uncertainty form this source was an orthogonal design. Table A1.5 summarizes the input values for Eq. (A1-13) and the corresponding estimates for $u_c(\Delta Q)$ at T_m levels of 281 K, 297 K, and 313 K. Under steady-state test conditions, the input estimates for x_1 and x_2 are nearly zero. The standard uncertainties $u\,(x_1)$ and $u\,(x_2)$ were estimated to be ±0.01 K (converted to microvolts in Table

A1.4 for the guard gap thermopile voltage), and ±0.5 K, respectively. The input values for b_i and $u(b_i) = s(b_i)$ were obtained from Table A1.4.

Table A1.5. Estimates for $u_c(\Delta Q)$

T_m (K)	x_1 (μV)	$u(b_1)$ (W/μV)	b_1 (W/μV)	$u(x_1)$ (μV)	x_2 (K)	$u(b_2)$ (W/K)	b_2 (W/K)	$u(x_2)$ (K)	$u_c(\Delta Q)$ (W)
281	-0.0230	3.94×10^{-5}	0.002 245	2.41	0.0051	3.95×10^{-4}	0.005 82	0.5	0.0061
281	-0.0374	3.94×10^{-5}	0.002 245	2.41	0.0058	3.95×10^{-4}	0.005 82	0.5	0.0061
281	0.0365	3.94×10^{-5}	0.002 245	2.41	0.0015	3.95×10^{-4}	0.005 82	0.5	0.0061
297	0.0298	2.39×10^{-5}	0.002 235	2.47	0.0008	2.39×10^{-4}	0.001 90	0.5	0.0056
297	0.1300	2.39×10^{-5}	0.002 235	2.47	-0.0043	2.39×10^{-4}	0.001 90	0.5	0.0056
297	0.0071	2.39×10^{-5}	0.002 235	2.47	0.0020	2.39×10^{-4}	0.001 90	0.5	0.0056
313	-0.0523	2.23×10^{-5}	0.002 363	2.54	0.0032	2.23×10^{-4}	0.001 34	0.5	0.0060
313	-0.0470	2.23×10^{-5}	0.002 363	2.54	-0.0038	2.23×10^{-4}	0.001 34	0.5	0.0060
313	-0.0375	2.23×10^{-5}	0.002 363	2.54	-0.0017	2.23×10^{-4}	0.001 34	0.5	0.0060

A1.3.3 Combined Standard Uncertainty *u* (*Q*)

The combined standard uncertainty $u(Q)$ was computed from Eq. (A1-14).

$$u_c(Q) = \sqrt{u^2(Q_m)_A + u^2(Q_m)_B + u^2(\Delta Q)} \tag{A1-14}$$

Table A1.6 summarizes the input values for Eq. (A1-14) and the corresponding estimates for $u_c(Q)$ at T_m levels of 281 K, 297 K, and 313 K.

Table A1.6. Combined standard uncertainty ($k = 1$) for $u_c(Q)$

T_m (K)	$u(Q_m)_A$ (W)	$u(Q_m)_B$ (W)	$u_c(\Delta Q)$ (W)	$u_c(Q)$ (W)	$\bar{Q}/2$ (W)	$u_{c,rel}(Q)$ (%)
281	0.000 67	0.0028	0.0061	0.0068	6.169	0.11
297	0.000 72	0.0030	0.0056	0.0064	6.456	0.10
313	0.000 72	0.0031	0.0060	0.0068	6.853	0.10

A1.4 Meter Area (*A*)

The meter area is the mathematical area through which the heat input to the meter plate Q_m flows normally under ideal guarding conditions (i.e., $Q_g \equiv 0$) into the specimen. The circular meter area, corrected for thermal expansion effects, was calculated from Eq. (A1-15):

$$A = \frac{\pi}{2}\left(r_o^2 + r_i^2\right)\times\left(1 + \alpha\Delta T_{mp}\right)^2 \tag{A1-15}$$

where r_o is the outer radius of the meter plate (m); r_i is the inner radius of the guard plate (m); α is the coefficient of thermal expansion of 6061-T6 aluminum (K^{-1}); and, ΔT_{mp} is the temperature difference of the meter plate (T_h) minus 20 °C (in kelvin).

A1.4.1 Plate Dimensions

The design dimensions for the meter plate and the guard plate diameters are 405.64 mm and 407.42 mm, respectively. A coordinate measuring machine (CMM) measured the roundness of the meter plate at six locations at the periphery and the diameter was determined to be 405.67 mm (within 0.03 mm of the design dimension). A uniform gap width of 0.89 mm was established using three precision pin gages spaced between the meter plate and guard plate at equiangular intervals. The uncertainty of the pin gages was +0.005 mm/–0.000 mm. Based on these check measurements, the input values for r_o and r_i for Eq. (A1-15) were determined to be 0.20282 m and 0.20371 m, respectively, and the standard uncertainty ($k = 1$) for both input values was taken to be 0.0254 mm.

A1.4.2 Thermal Expansion Effects

For α, an input value of 23.6×10^{-6} K^{-1} at 20 °C was obtained from aggregated handbook data [20] for 6061-T6 aluminum. The standard uncertainty ($k = 1$) for the value of α was estimated conservatively to be 10 % (2.36×10^{-6} K^{-1}). The standard uncertainty ($k = 1$) for ΔT_{mp} was based the uncertainty for the plate temperature (Sec. A1.6.7).

A1.4.3 Combined Standard Uncertainty *u* (*A*)

Application of Eq. (A1-3) to Eq. (A1-15) yields

$$u_c(A) = \sqrt{c_{r_0}^2 u^2(r_o) + c_{r_i}^2 u^2(r_i) + c_\alpha^2 u^2(\alpha) \; + c_{\Delta T_{mp}}^2 u^2(\Delta T_{mp})} \qquad \text{(A1-16)}$$

with

$$c_{r_o} = \frac{\partial A}{\partial r_o} = \pi r_o \left(1 + \alpha \Delta T_{mp}\right)^2$$

$$c_{r_i} = \frac{\partial A}{\partial r_i} = \pi r_i \left(1 + \alpha \Delta T_{mp}\right)^2$$

$$c_\alpha = \frac{\partial A}{\partial \alpha} = \pi \Delta T_{mp} \left(r_o^2 + r_i^2\right) \times \left(1 + \alpha \Delta T_{mp}\right)$$

$$c_{\Delta T_{mp}} = \frac{\partial A}{\partial \left(\Delta T_{mp}\right)} = \pi \alpha \left(r_o^2 + r_i^2\right) \times \left(1 + \alpha \Delta T_{mp}\right)$$

Table A1.6 summarizes the contributory uncertainties for the meter-area calculation.

Table A1.6. Standard uncertainty components ($k = 1$) for A

Source	Description	Estimate	Standard Uncertainty	Type of Evaluation
$u_1(r_o)$	Meter-plate outer radius	202.82 mm	0.0254 mm	B
$u_2(r_i)$	Guard-plate inner radius	203.71 mm	0.0254 mm	B
$u_3(\alpha)$	Linear thermal expansion coefficient	23.6×10^{-6} K^{-1}	2.36×10^{-6} K^{-1}	B
$u_4(\Delta T_{mp})$	Temperature difference ($T_m = 280$ K)	–0.65 K	0.063 K	B
$u_4(\Delta T_{mp})$	Temperature difference ($T_m = 310$ K)	29.4 K	0.063 K	B
$u_4(\Delta T_{mp})$	Temperature difference ($T_m = 340$ K)	59.4 K	0.063 K	B

Table A1.7 summarizes the combined standard uncertainties for A at three levels of T_m. Values of A were computed with Eq. (A1-15). The estimates for $u_c(A)$ are, as evident in Table A1.7, quite small.

Table A1.7. Combined standard uncertainty ($k = 1$) for $u_c(A)$

T_m (K)	A (m^2)	$u_c(A)$ (m^2)	$u_{c,rel}(A)$ (%)
281	0.12979	0.000023	0.018
297	0.12988	0.000025	0.019
313	0.12998	0.000029	0.023

A1.5 In-situ Thickness (L)

The thickness of each pair of specimens was measured during testing using the average of eight (four top and four bottom) linear positioning transducers at the periphery of the plates. The equation for the *in-situ* thickness measurement is:

$$L = \frac{1}{n}\sum_{i=1}^{n} L_i \qquad \text{(A1-17)}$$

where L_i is the measurement value for an individual positioning system and n equals 8.

Each positioning system consists of a digital readout and a slider translating on a tape scale bonded to a precision ground plate of a low thermal expansion iron-nickel (FeNi36) alloy. The electrical windings on the scale are inductively coupled with the slider and the resulting output signal from the scale is resolved by the digital readout having a resolution of 2.54×10^{-6} m. The digital readouts are reset by placing one set of fused-quartz spacers of known thickness between the cold plate and hot plate. Fused-quartz was selected for the spacers because of its extremely low coefficient of thermal expansion, 5.5×10^{-7} cm/cm·K.

The standard uncertainties associated with the mean of the eight linear positioning transducers were determined for each guarded-hot-plate test using Eq. (A1-5) where n was equal to 8. The standard uncertainty $u(L)_A$ was subsequently computed from the pooled experimental standard deviations for the 15 tests and found to be 0.0508 mm. Contributory uncertainty components for the thickness measurement are described below. The contributory uncertainty for the gage blocks was 35 nm and neglected in further analysis.

A1.5.1 Fused-quartz Spacers, $u_1(L)_A$

The standard uncertainty was computed from the pooled standard deviations of multiple measurement locations of the four fused-quartz spacers and was 0.00422 mm ($k = 1$).

A1.5.2 Micrometer, $u_2(L)_B$

The standard uncertainty for the micrometer used to determine the lengths of the fused-quartz spacers was based on a uniform rectangular distribution with a symmetrical half-

width a of 0.0025 mm. Substitution of the half-width in Eq. (A1-9) yields a standard uncertainty of 0.0015 mm ($k = 1$).

A1.5.3 Linear Positioning System, $u_3\,(L)_B$

The standard uncertainty for the linear position transducers was based on the accuracy specification from the manufacturer as 0.0051 mm ($k = 1$).

A1.5.4 Repeatability of Linear Positioning System, $u_4\,(L)_A$

The short-term repeatability of the linear positioning system was determined from a sequence of replicate thickness measurements taken over four days using the fused-quartz spacers as reference values. The linear positioning indicators for the cold plates were initially reset using the four fused-quartz spacers. The cold plates were subsequently opened and closed until the plates were in complete contact again with the spacers. The readings from the digital indicators were recorded and the procedure was repeated five times (per day). To check the variation from day to day, readings were taken over four days for a total of twenty thickness averages. Table A1.8 gives summary statistics for the short-term repeatability test.

Table A1.8. Summary statistics for short-term repeatability of linear positioning system

Day	Replicates	Day average (m)	Within-day standard deviation (m)
1	5	1.266×10^{-2}	4.98×10^{-6}
2	5	1.268×10^{-2}	5.88×10^{-6}
3	5	1.267×10^{-2}	1.99×10^{-6}
4	5	1.267×10^{-2}	5.09×10^{-6}

The standard deviation of the daily averages (s_a) was 7.91×10^{-6} m and the (pooled) within-day standard deviation (s_d) was 4.72×10^{-6} m. The standard uncertainty was determined to be 8.97×10^{-6} m using Eq. (A1-18) from [21]:

$$u_4\left(L\right) = \sqrt{s_a^2 + \frac{r-1}{r} s_d^2} \tag{A1-18}$$

where r is equal to the number of replicates per day. The DoF (degrees of freedom) was determined from the Welch-Satterthwaite formula in Ref. [14].

A1.5.5 Plate Flatness, $u_5\,(L)_A$ and $u_6\,(L)_B$

The standard uncertainty associated with the mean of 32 thickness measurements of the meter plate was determined to be 0.0023 mm. The standard uncertainty for the coordinate measuring machine (CMM) used to determine the meter-plate thickness was based on the accuracy specification from the manufacturer as 0.0051 mm ($k = 1$). The standard uncertainty for the plate flatness was estimated from Eq. (A1-19) to be 0.0079 mm.

$$u_{c,56}(L) = \sqrt{2 \times \left(u_5^2(L)\right) + u_6^2(L)} \tag{A1-19}$$

A1.5.6 Plate Deflection, $u_7(L)_B$

The mechanical deflection of the (large) cold plates under mechanical loading was evaluated as a Type B uncertainty using classical stress and strain formulae for flat plates. Clamping forces (F_1 and F_2) were transmitted axially (Fig. 8) and distributed over a circular area at the center of each cold plate. For a uniform load over a concentric circular area of radius r_f, the maximum deflection y_{max} at the center of the cold plate is given by the following formula [22]. Uniform support loading was assumed because the test specimen was a semi-rigid material.

$$u_7(L) = y_{\max} = -\frac{3F(m^2-1)}{16\pi E m^2 t_c^3}\left[4r_f^2 \ln\frac{r_f}{r_p} + 2r_f^2\left(\frac{3t_c+1}{t_c+1}\right) + \frac{r_f^4}{r_p^2} - r_f^2\left(\frac{7t_c+3}{t_c+1}\right) + \frac{\left(r_p^2-r_f^2\right)r_f^4}{r_p^2 r_f^2}\right] \tag{A1-20}$$

where:

F = applied load (N);
m = reciprocal of Poisson's ratio (dimensionless);
E = modulus of elasticity ($N \cdot m^{-2}$);
t_c = thickness of cold plate (m); and,
r_p = radius of (cold) plate (m).

From Table 8, the average clamping pressure f for the guarded-hot-plate tests was 1.1 kPa resulting in an applied load of approximately 477 N. For aluminum alloy 6061-T6, the values for m and E were taken to be $(0.33)^{-1} = 3.0$ and 6.9×10^7 kPa, respectively. The cold plate thickness was 25.4 mm; radius of uniform loading was 108 mm; and, the cold plate radius was 508 mm. Substituting these values into Eq. (A1-20), yields a value of 0.032 mm for y_{max}. A major limitation for this assessment approach is that the cold plate is not a solid plate, but is actually a composite construction to allow the flow of coolant internally within the plate.

A1.5.7 Combined Standard Uncertainty $u(L)$

Table A1.9 summarizes the contributory uncertainties $u_i(L)$ for the thickness measurement.

Table A1.9. Standard uncertainty components ($k = 1$) for L

Source	Description	Standard Uncertainty (mm)	Type of Evaluation
$u(L)_A$	Multiple measurement locations	0.0508	A
---	Gage block calibration	Negligible	B
$u_1(L)$	Fused-quartz spacers – multiple measurements	0.0042	A
$u_2(L)$	Fused-quartz spacers – micrometer	0.0015	B
$u_3(L)$	Linear positioning system	0.0051	B
$u_4(L)$	Repeatability of linear positioning system	0.0090	A
$u_{c,5,6}(L)$	Plate flatness	0.0079	B
$u_7(L)$	Cold plate deflection	0.032	B

Equation (A1-21) computes the combined standard uncertainty (k = 1) for the temperature measurement.

$$u_c(L) = \sqrt{u^2(L)_A + \sum_{i=1}^{7} u_i^2(L)} \quad \text{(A1-21)}$$

Substituting the component standard uncertainties from Table A1.9 into Eq. (A1-21) yields a value of 0.061 mm. For L equal to 13.43 mm (Table 8), $u_{c,\,rel}$ (L) was equal to 0.46 %.

A1.6 Temperature Difference (ΔT)

The temperature difference of the specimens was determined from the following equation:

$$\Delta T = T_h - T_c = T_h - \left(T_{c1} + T_{c2}\right)/2 \quad \text{(A1-22)}$$

where the subscripts h and c refer to hot and cold, respectively, and the subscripts 1 and 2 refer to the two cold plates (Fig. 8).

The temperature difference across the specimen is determined by small capsule industrial platinum resistance thermometers (PRTs) located in the hot and cold plates (T_h and T_c, respectively). Each thermometer is constructed of a strain-free platinum element supported in a gold-plated copper cylinder 3.18 mm in diameter by 9.7 mm long backfilled with helium gas and hermetically sealed. The operational range is from –260 °C to 260 °C and the nominal electrical resistance is 100 Ω at 0 °C. The electrical resistance of each 4-wire PRT is measured with integrating digital voltmeter (DVM).

The standard uncertainties $u\,(\Delta T_i\,)_A$ associated with the time-averaged observations taken over the steady-state measurement period were determined using Eq. (A1-5) where n was equal to 120. The standard uncertainty $u\,(\Delta T\,)_A$ was subsequently computed from the pooled experimental standard deviations for the 15 tests and found to be 0.0002 K which, in comparison to other temperature uncertainty estimates, was neglected.

A1.6.1 Sensor Calibration $u_1\,(T\,)_B$

The expanded uncertainty (k = 2) for the bath temperature measurements for the meter-plate PRT calibration was reported to be 0.01 K. Therefore, the standard uncertainty estimate of 0.005 °C (k = 1) was used for the uncertainty analysis.

A1.6.2 Regression Analysis $u_2\,(T\,)_A$

For each PRT, the individual observations (in ohms) were converted to temperature with the curve fit for the NIST Thermometry calibration data. The standard uncertainty was computed from the pooled residual standard deviations for each curve fit of the calibration data and was 0.0052 K (k = 1).

A1.6.3 Electrical Resistance Measurement $u_3\,(T)_B$

The standard uncertainty for electrical resistance measurement of the PRT was based on the 1 year manufacturer specification for the integrating voltmeter (DVM). A uniform rectangular distribution was assumed for the accuracy specification with a symmetrical half-width *a* computed from Eq. (A1-23) where *reading* is in ohms.

$$300\ \Omega\ \text{Range}: \ a = 0.00015 \times reading \ + \ 8\ \text{m}\Omega \ + \ 0.0001 \times reading \qquad \text{(A1-23)}$$

For a *reading* of 131.372 Ω, $a_{300\Omega}$ is 0.041 Ω. Substitution of 131.372 Ω ± (0.041 Ω/2) in the PRT calibration curve fit, yields a corresponding temperature half-width of 0.105 K. Final substitution of the half-width of 0.105 K in Eq. (A1-9) yields a standard uncertainty of 0.0607 K.

A1.6.4 Temperature Rise due to PRT Self-heating $u_4\,(T)_B$

The nominal 100 Ω PRT dissipates about 0.0001 W for a 1 mA excitation current. For the cold plate PRTs, the thermal conductance of the metal-to-air-to-metal interface between sensor and plate is estimated to be 0.058 W/K. Thus, the temperature rise (0.0001 W÷0.058 W/K) is 0.0017 K. For the meter-plate PRT, a thin layer of thermally conductive silicone paste was applied to the sensor exterior surface to improve thermal contact.

A1.6.5 Radial Plate Temperature Variation $u_5\,(T)_B$

From previous measurement data [23], an estimate for the radial sampling uncertainty was taken to be 0.015 K. In these separate experiments, the temperature profiles of the meter plates were estimated utilizing independent thermopile constructions placed between the plate surfaces and semi-rigid specimens.

A1.6.6 Axial Plate Temperature Variation $u_6\,(T)_B$

A rigorous analytical analysis by Peavy published in Hahn et al. [24] shows that, for typical specimen insulations, the differences between the temperature of the meter-plate PRT at the mid-plane of the guard gap and the average surface temperature of the meter plate is less than 0.01 % and, thus, neglected in further analyses.

A1.6.7 Combined Standard Uncertainty $u\,(T)$

Table A1.10 summarizes the standard uncertainty sources $u_i\,(T)$, their descriptions, and corresponding uncertainty estimates for the PRT temperature measurement.

Equation (A1-24) computes the combined standard uncertainty (k = 1) for the temperature measurement.

$$u_c\left(T\right) = \sqrt{\sum_{i=1}^{6} u_i^2\left(T\right)} \qquad \text{(A1-24)}$$

Annex 1

Table A1.10. Standard uncertainty components ($k = 1$) for T

Source	Description	Standard Uncertainty (K)	Type of Evaluation
$u(T)_A$	Repeated observations	Negligible	A
$u_1(T)$	PRT calibration by NIST Thermometry Group	0.005	B
$u_2(T)$	PRT calibration data curve fit	0.0051	A
$u_3(T)$	Electrical resistance measurement/conversion	0.0607	B
$u_4(T)$	Temperature rise due to PRT self-heating	0.0017	B
$u_5(T)$	Temperature variation - radial dimension	0.015	B
$u_6(T)$	Temperature variation - axial dimension	Negligible	B

Substituting the standard uncertainty components from Table A4-7 into Eq. (A1-24) yields a value of 0.063 K.

A1.6.8 Combined Standard Uncertainty $u(\Delta T)$

For a double-sided guarded-hot-plate test, the temperature difference (ΔT) across the specimen pair was determined from Eq. (A1-25).

$$\Delta T = T_h - \left(T_{c1} + T_{c2}\right)/2 \tag{A1-25}$$

Applying Eq. (A1-3) to Eq. (A1-25) and setting $u(T_h) = u(T_{c1}) = u(T_{c2}) = u(T)$ yields

$$\boxed{u_c\left(\Delta T\right) = \sqrt{\frac{3}{2} \times u^2\left(T\right)} = \sqrt{1.5 \times 0.063^2} = 0.077\,\mathrm{K}} \tag{A1-26}$$

For ΔT equal to 20.000 K (Table 8), $u_{c,\,rel}(\Delta T)$ was equal to 0.39 %.

A1.6.9 Combined Standard Uncertainty $u(T_m)$

The mean temperature was determined from the Eq. (A1-27)

$$T_m = \frac{\left(T_h + T_c\right)}{2} = \frac{T_h + \left(T_{c1} + T_{c2}\right)/2}{2} = \frac{T_h}{2} + \frac{T_{c1}}{4} + \frac{T_{c2}}{4} \tag{A1-27}$$

Applying Eq. (A1-3) to Eq. (A1-27) and setting $u(T_h) = u(T_{c1}) = u(T_{c2}) = u(T)$ yields

$$\boxed{u_c\left(T_m\right) = \sqrt{\frac{6}{16} \times u^2\left(T\right)} = \sqrt{0.375 \times 0.063^2} = 0.039\,\mathrm{K}} \tag{A1-28}$$

Annex 2

Annex 2 - Uncertainty Analysis for Bulk Density (ρ)

A2.1 Digital Balance Uncertainty

The basic measurement equation for the digital balance is: *Indication = Applied load ± Uncertainty*. Assuming a uniform (rectangular) distribution, the standard uncertainty and the process standard deviation (s_p) for the balance were determined from Eq. (A2-1).

$$u_{c,bal} = s_p = \frac{d}{\sqrt{3}} \tag{A2-1}$$

where d is equal to one display unit (i.e., the resolution) of the balance. For d equal to 0.1 g, $u_{c,bal}$ is determined to be 0.058 g.

A2.2 Length Uncertainties

The Type A standard uncertainties for the length measurements were computed by pooling the standard deviations from a relatively small number of measurements for each (square) specimen or metered section cylinder.

The Type B standard uncertainties for the length measurements were assumed to have a uniform distribution in the interval ±a; where ±a was the smallest length interval of the length scale. The values of the interval ±a for the steel rule, calipers, and height gage were 0.5 mm, 0.01 mm, and 0.1 mm, respectively. The standard uncertainties were computed using Eq. (A2-1) with a set equal to d.

A2.3 Uncertainty Budget

Table A2.1 summarizes the Type A and Type B standard uncertainties for the determination of bulk density for the 30 specimens (Sec. 4.3).

Table A2.1. Summary of standard uncertainty components for bulk density

Source	$u(x_i)$, $k = 1$ (Type A or Type B)		DoF[a] for Type A evaluation or Type B source	
	Specimen	Cylinder		
1) Digital balance (m)	0.058 g (B)	0.058 g (B)	Eq. (A2-1)	Eq. (A2-1)
2) Length measurement (l)				
Repeated measurements	0.01 mm (A)	0.67 mm (A)	180	16
Steel rule	0.29 mm (B)	0.29 mm (B)	Eq. (A2-1)	Eq. (A2-1)
3) Thickness measurement (L)				
Repeated measurements	0.005 mm (A)	0.039 mm (A)	150	40
Height gage	0.058 mm (B)	0.058 mm (B)	Eq. (A2-1)	Eq. (A2-1)
Datum surface (granite plate)	0.015 mm (B)	0.015 mm (B)	Mfg.	Mfg.

[a] Degrees of freedom

Annex 2

A2.4 Combined Standard Uncertainty

A2.4.1 Square Specimen Geometries

For square geometries, Eqs. (1) and (5) are re-written as

$$\rho_s = \frac{m}{l_1 \times l_2 \times L} \tag{A2-2}$$

where l_1 and l_2 are the length and width, respectively, of the specimen. For equal length sides, l_1 and l_2 are equal to l.

The combined standard uncertainty $u_c(\rho)$ was determined using the following equation

$$u_c(\rho_s) = \sqrt{c_m^2 u^2(m) + 2[c_l^2 u^2(l)] + c_L^2 u^2(L)} \tag{A2-3}$$

with

$$c_m = \frac{\partial \rho_s}{\partial m} = \frac{1}{l^2 L}$$

$$c_l = \frac{\partial \rho_s}{\partial l} = \frac{-m}{l^3 L}$$

$$c_L = \frac{\partial \rho_s}{\partial L} = \frac{-m}{l^2 L^2}$$

The factor 2 in Eq. (A2-3) occurs to account for the two equal sides of the specimen. Average values for c_m, c_l, c_L, were 172.3 m^{-3}, -61.5 kg/m^4, and -3007 kg/m^4, respectively. Substituting the uncertainty values for the specimen from Table A2.1 into Eq. (A2-3), the combined standard uncertainty $u_c(\rho_s)$ for the specimen bulk density determination was determined from the following equation:

$$u_c(\rho_s) = \sqrt{\begin{array}{l}(172.3)^2 \times \left(\frac{0.058}{1000}\right)^2 + 2 \times \left[(-61.5)^2 \times \left(\frac{0.29}{1000}\right)^2\right] + \\ +(-3007)^2 \times \left[\left(\frac{0.005}{1000}\right)^2 + \left(\frac{0.058}{1000}\right)^2 + \left(\frac{0.015}{1000}\right)^2\right]\end{array}} \tag{A2-4}$$

$$\boxed{u_c(\rho_s) = \sqrt{(9.987 + 63.62 + 3268) \times 10^{-5}\ \mathrm{kg^2/m^6}} = 0.18\ \mathrm{kg/m^3}} \tag{A2-5}$$

Annex 2

A2.4.2 Circular Specimen Geometry

For a circular geometry, Eq. (12) is re-written as

$$\rho_m = \rho_{cyl} = \frac{m}{\left(\pi r^2\right)\times L} = \frac{4m}{\left(\pi d^2\right)\times L} \tag{A2-6}$$

where r and d ($d = 2 \times r$) are the radius and diameter, respectively, of the cylinder.

The combined standard uncertainty u_c (ρ_{cyl}) was determined using the following equation

$$u\left(\rho_m\right) = u_c\left(\rho_{cyl}\right) = \sqrt{c_m^2 u^2\left(m\right) + c_c^2 u^2\left(d\right) + c_L^2 u^2\left(L\right)} \tag{A2-7}$$

with

$$c_m = \frac{\partial \rho_{cyl}}{\partial m} = \frac{4}{\pi d^2 L}$$

$$c_d = \frac{\partial \rho_{cyl}}{\partial d} = \frac{-8m}{\pi d^3 L}$$

$$c_L = \frac{\partial \rho_{cyl}}{\partial L} = \frac{-4m}{\pi d^2 L^2}$$

Average values for c_m, c_d, c_L, were 589.3 m^{-3}, -208.8 kg/m^4, and -3103 kg/m^4, respectively. Substituting the uncertainty values for the cylinder from Table A2.1 into Eq. (A2-7), the combined standard uncertainty u_c (ρ_{cyl}) for the meter area bulk density determination was determined from the following equation:

$$u\left(\rho_m\right) = u_c\left(\rho_{cyl}\right) = \sqrt{\begin{array}{l}\left(589.3\right)^2 \times \left(\frac{0.058}{1000}\right)^2 + \left(-208.8\right)^2 \times \left[\left(\frac{0.67}{1000}\right)^2 + \left(\frac{0.29}{1000}\right)^2\right] + \\ + \left(-3103\right)^2 \times \left[\left(\frac{0.039}{1000}\right)^2 + \left(\frac{0.058}{1000}\right)^2 + \left(\frac{0.015}{1000}\right)^2\right]\end{array}} \tag{A2-8}$$

$$\boxed{u\left(\rho_m\right) = u_c\left(\rho_{cyl}\right) = \sqrt{\left(116.8 + 2324 + 4920\right)\times 10^{-5}\ \mathrm{kg^2/m^6}} = 0.27\ \mathrm{kg/m^3}} \tag{A2-9}$$

A2.4.3 Metered Section Correction for Specimen Pair

Application of Eq. (A1-3) to Eq. (14) yields:

$$u_c\left(\rho_{pair,\,corr}\right) = \sqrt{c_{\rho_{s1}}^2 u^2\left(\rho_{s1}\right) + c_{\rho_{s2}}^2 u^2\left(\rho_{s2}\right) + c_{\rho_m}^2 u^2\left(\rho_m\right) + c_{\rho_s}^2 u^2\left(\rho_s\right) + s^2\left(\overline{\rho}\right)} \tag{A2-10}$$

with

$$c_{\rho_{s,1}} = c_{\rho_{s,2}} = \frac{\partial\left(\rho_{pair,corr}\right)}{\partial\rho_{s,1}} = \frac{1}{2}$$

$$c_{\rho_m} = c_{\rho_s} = \frac{\partial\left(\rho_{pair,corr}\right)}{\partial\rho_m} = 1$$

$$s^2\left(\overline{\rho}\right) = \frac{s^2\left(\rho_i\right)}{n}$$

Substituting the above sensitivity values (c_i), the standard uncertainties from Eqs. (A2-5) and (A2-9), and the experimental standard deviation (s) and n from Table 10 yields:

$$u_c\left(\rho_{pair,corr}\right) = \sqrt{\left[\frac{(0.18)^2}{4} + \frac{(0.18)^2}{4} + (0.27)^2 + (0.18)^2 + \frac{(0.67)^2}{8}\right] \mathrm{kg^2/m^6}}$$

$$u_c\left(\rho_{pair,corr}\right) = 0.42\ \mathrm{kg/m^3} \qquad \text{(A2-11)}$$

A2.5 Effect of Buoyant Force

Corrections for the effect of the buoyant force on the polystyrene solid polymer were estimated to be 0.1 % and neglected.

Annex 3 - Compressive Resistance of Expanded Polystyrene Foam

The compressive resistance of SRM 1453 was determined in accordance with ASTM Test Method C 165 [25], Procedure A, using a universal testing machine. The purpose was to provide users of SRM 1453 a maximum pressure limit before the material would mechanically yield, i.e., deform permanently. Seven cylindrical specimens, 100 mm in diameter by 13 mm thick, were cut from Board 049 and conditioned in an environment of (23 ± 0.8) °C and (53 ± 0.2) % relative humidity (aqueous salt solution) for about 11 days to a steady mass. Since the compressive resistance is a function of bulk density, the specimens were specifically selected from the lowest densities available. That is, the measured compressive resistance would be expected to represent the low end of the range of the SRM.

During testing, the machine was operated at a crosshead speed of 1 mm/min. The compressive load and corresponding deformation were sampled in real-time at a rate of 9.1 points per second in order to construct a load-deformation curve for each specimen. Using a straightedge, the straight portion of the curve was extended to the *x*-axis, establishing a "zero deformation point". All deformations were determined with respect to this (zero) point. The compressive resistance was determined from:

$$S = \frac{W}{A} \tag{A3-1}$$

where;

W = compressive load at a given deformation, N; and,
A = original (undeformed) area, m^2.

The compressive resistance for the 7 specimens at an average deformation of 0.34 mm (2.5 %) is summarized in Table A3.1. The load-deformation curve departed from linearity above this deformation.

Annex 3

Table A3.1. Compressive resistance of specimens of SRM 1453, Expanded Polystyrene Board

ID	Bulk density (kg/m^3)	Undeformed area (m^2)	Deformation (mm)	Strain (%)	Load (N)	Compressive resistance (kPa)
1	31.3	0.00785	0.34	2.5	2474	315.0
2	32.6	0.00778	0.27	2.0	2275	292.6
3	30.8	0.00781	0.33	2.5	2121	271.4
4	31.8	0.00781	0.38	2.8	2469	316.0
5	32.2	0.00785	0.35	2.6	2667	339.6
6	31.2	0.00785	0.35	2.6	2375	302.4
7	29.5	0.00785	0.36	2.7	2307	293.7
Mean	31.3	0.00783	0.34	2.5	2384	304.4
Std. dev.	1.0	0.00003	0.03	0.3	175	21.7

Annex 4

Annex 4 – Bayesian Errors in Variables Analysis

A4.1 Nomenclature (specific to Annex 4)

Symbol	Description
$\hat{T}_{m,i}$	mean measured temperature at which thermal conductivity for specimen pair i is measured
$T_{m,i}$	true unknown mean temperature at which thermal conductivity for specimen pair i is measured
β_i	regression parameters
$\lambda_{\text{exp},\,i}$	measured thermal conductivity of specimen pair i
$\lambda_{\text{true},\,i}$	true unknown thermal conductivity of specimen pair i
$\hat{\rho}_{\,pair,corr,i}$	corrected mean measurement of bulk density for specimen pair i
ρ_i	true unknown mean bulk density for specimen pair i

A4.2 Background

The quantities $\lambda_{\text{exp},i}$, $\hat{T}_{m,i}$, and $\hat{\rho}_{pair,corr,i}$ can be thought of as approximations to their true unknown counterparts[5]. The following model for the measurements, which explicitly relates the measurements to their true unknown counterparts, is employed.

$$\begin{aligned} \lambda_{\text{exp},i} &\sim N\left(\lambda_{\text{true},i}, 3.61\times10^{-8}\right) \\ \hat{T}_{m,i} &\sim N\left(T_{m,i}, 0.0015\right) \\ \hat{\rho}_{\,pair,corr,i} &\sim N\left(\rho_i, 0.1764\right) \\ \lambda_{\text{true},i} &\sim N\left(\beta_0 + \beta_1\rho_i + \beta_2 T_{m,i}, \sigma^2\right) \end{aligned} \tag{A4-1}$$

The variances for the normal distributions governing $\hat{T}_{m,i}$ and $\hat{\rho}_{pair,corr,i}$ are given in Eq. (A1-28) and Eq. (A2-11), respectively. The variance for the normal distribution governing $\lambda_{exp,i}$ can be derived by applying Eq. (A1-3) to Eq. (3) using the quantities from Eq. (9), which are derived in Annex 1.

Inference for the parameters of (A4-1) (T_i, ρ_i, β_0, β_1, β_2, and σ) is performed under the Bayesian paradigm, so priors are assigned to them. The following priors are used:

[5] In accordance with the International vocabulary of basic and general terms in metrology (known as the VIM), a true value "in the classical approach to describing measurement, is considered unique and, in practice, unknowable".

Annex 4

$$
\begin{aligned}
T_i &\sim N\left(300, \frac{50}{3}\times\frac{50}{3}\right) \\
\rho_i &\sim N\left(40, \frac{10}{3}\times\frac{10}{3}\right) \\
\beta_0, \beta_1, \text{ and } \beta_2 &\sim N\left(0, 1.0\times10^5\right) \\
\sigma &\sim \text{Half-Cauchy}\left(0, 25\right)
\end{aligned}
\tag{A4-2}
$$

The Half-Cauchy(0, 25) may be thought of in the following way.

$$
\begin{aligned}
X &\sim N\left(0, 25^2\right) \\
Y &\sim \chi_1^2 \\
\sigma &= \frac{|X|}{\sqrt{Y}}
\end{aligned}
\tag{A4-3}
$$

This specific Half-Cauchy distribution as a prior for a standard deviation is proposed in [26]. The means for the prior distributions on T_i and ρ_i are chosen to be the approximate center of the measured values. The variances for the prior distributions on T_i and ρ_i are chosen so that 50 and 10, respectively, represent 3 standard deviations. The selection of 3 standard deviations is an arbitrary choice. The sensitivity of the results to this choice was examined, and under reasonable choices (i.e. reasonably diffuse priors) the results were not affected. The values 50 and 10 encompass the range of the temperature and bulk density measurements, respectively.

A4.3 Calculations

All calculations of posterior summaries were done using the open-source software[2] OpenBUGS [27] and R [28]. The posterior means of β_0, β_1, and β_2 are 0.00111, -0.0000424, and 0.000115, respectively. Thus, given a new measurement of temperature and density, $\hat{T}_{m,new}$ and $\hat{\rho}_{pair,corr,new}$, respectively, the prediction of measured thermal conductivity, $\tilde{\lambda}_{exp,new}$ is

$$
\tilde{\lambda}_{\text{exp,new}} = 0.00111 - 0.0000424\,\hat{\rho}_{pair,corr,new} + 0.000115\,\hat{T}_{m,new} \tag{A4-4}
$$

A4.4 Uncertainty

Since the uncertainty in predictions from Eq. (A4-4) can depend on the specific $T_{m,new}$ and $\rho_{pair,corr,new}$, a regular grid (10×10) of $(\hat{T}_{m,new,j}, \hat{\rho}_{pair,corr,new,j})$ pairs over $\left[\min\{\hat{T}_{m,i}\}, \max\{\hat{T}_{m,i}\}\right] \times \left[\min\{\hat{\rho}_{pair,corr,i}\}, \max\{\hat{\rho}_{pair,corr,i}\}\right]$ is constructed. Note that i = 1, 2, …, 15 indexes the original 15 measurements, and j = 1, 2, …, 100 indexes the rectangular grid. Then, the posterior predictive distribution of $\lambda_{exp,new,j}$ a new NIST measurement of thermal conductivity at $(\hat{T}_{m,new,j}, \hat{\rho}_{pair,corr,new,j})$, treating $(\hat{T}_{m,new,j}, \hat{\rho}_{pair,corr,new,j})$ as measured values, is calculated for each point in the grid

$j = 1, 2, \ldots, 100$. We calculate the posterior predictive distribution of $\lambda_{exp,new,j}$ instead of $\lambda_{true,new,j}$ to ensure that our final expanded uncertainty accounts for the known sources of uncertainty, including those described in Annexes 1 and 2. Thus, the uncertainty is interpreted in terms of a new NIST measurement instead of the unknown true value. The posterior predictive distributions are then used to construct 95% credible intervals for $\lambda_{exp,new,j}$, and the upper and lower bounds of those intervals are denoted as $\lambda^{u}_{exp,new,j}$ and $\lambda^{l}_{exp,new,j}$, respectively. The relative expanded uncertainty for a prediction from Eq. (A4-4) is then taken to be

$$U = \underbrace{\max}_{j}\left\{\underbrace{\max}_{l,u}\left\{\frac{\tilde{\lambda}_{\mathrm{exp,new},j} - \lambda^{l}_{\mathrm{exp,new},j}}{\tilde{\lambda}_{\mathrm{exp,new},j}}, \frac{\lambda^{u}_{\mathrm{exp,new},j} - \tilde{\lambda}_{\mathrm{exp,new},j}}{\tilde{\lambda}_{\mathrm{exp,new},j}}\right\}\right\} = 1.5\ \% \qquad \text{(A4-5)}$$

where

$$\tilde{\lambda}_{\mathrm{exp,new},j} = 0.00111 - 0.0000424\,\hat{\rho}_{pair,corr,new,j} + 0.000115\,\hat{T}_{m,new,j}. \qquad \text{(A4-6)}$$

Of course for some *j*, *U* will represent a credible interval that covers more than 95 % of the appropriate posterior predictive distribution, but to give a single expanded uncertainty for all predictions from Eq. (A4-4) that must be the case. The effective value of *k* for this expanded uncertainty is 2, which is calculated by dividing *U* by the standard deviation of the posterior predictive distribution of $\lambda_{exp,new,j}$ that provides *U*.

Annex 5

Annex 5 - Sorption Isotherms for Expanded Polystyrene Foam

Sorption isotherms for expanded polystyrene foam were determined using fixed-point humidities provided by aqueous salt solutions. To increase the surface area and thus enhance the sorption process, small rectangular billets, 0.5 mm by 2 mm by 13 mm, of foam were cut. One set of billets was prepared for adsorption measurements; the other for desorption measurements. Both sets of foam billets were conditioned in an environment over calcium-chloride desiccant to obtain a "dry" or tare mass. The billets for desorption were subsequently removed from the desiccant containers and placed over distilled water. A fixed number of billets from each set were subsequently placed in containers at 11 %, 33 %, 43 %, 58 %, 79 %, 84 %, 94 % and 97 % relative humidity at laboratory temperature of 24 °C.

The billets from each container were collectively removed and weighed to monitor changes in mass due to sorption of water vapor. The weighing process was repeated until the conditioned mass of the billets achieved a steady value (i.e., less than 1 % change over a 2-day interval). The equilibrium moisture content, $\gamma(\varphi)$, was determined by taking the differences between the conditioned mass, $m(\varphi)$, and initial mass, m_i, and dividing by m_i.

$$\gamma(\varphi) = \frac{m(\varphi) - m_i}{m_i} \tag{A4-1}$$

For the relative humidity range of 11 % to 94 %, $\gamma(\varphi)$ was found to be less than 0.4 % and less than 1 % at 97 % relative humidity.

Annex 6 - General Precautions for Expanded Polystyrene Foam

A6.1 Upper Temperature Limit

Polystyrene is a thermoplastic and, by definition, has a well-defined temperature at which the polymer softens. The upper temperature limit before cellular polystyrene foam softens, as specified in the ASTM Specification C 578 [12], is 74 °C. Mehta et al. [29] reported that similar polymer polystyrene beads when exposed to elevated temperatures collapsed about 110 °C to 120 °C. The collapsed beads melted at 160 °C and began to vaporize above 275 °C [29].

A6.2 Flammability

Standard Reference Material 1453 is a commercial grade of expanded polystyrene foam that does not contain fire-retarding additives. It is an organic thermoplastic material that is combustible and, at elevated temperatures melts (at a temperature greater than 160 °C, [29]). Do not expose the material to sources of ignition.

A6.3 Solvents

Polystyrene is soluble in many organic solvents such as chlorinated and aromatic hydrocarbons, esters, and ketones. The aromatic chemical structure of polystyrene is inherently water repellant. As noted in Annex 5, the material is very insensitive to low levels of humidity.

A6.4 Ultraviolet Degradation

When exposed to sunlight (ultraviolet radiation), polystyrene degrades as evidenced by discoloration of the surface. To minimize degradation, protect SRM 1453 by covering when exposed to direct sunlight.